HHS Public Access

Author manuscript

Neuron. Author manuscript; available in PMC 2021 December 22.

Published in final edited form as:

Neuron. 2021 September 01; 109(17): 2767–2780.e5. doi:10.1016/j.neuron.2021.06.020.

Hippocampal ripples and their coordinated dialogue with the default mode network during recent and remote recollection

Yitzhak Norman[1,4,*], **Omri Raccah**[2], **Su Liu**[2], **Josef Parvizi**[2,3,4], **Rafael Malach**[1,3,4,5,*]

[1]Department of Neurobiology, Weizmann Institute of Science, Rehovot 76100, Israel

[2]Laboratory of Behavioral and Cognitive Neuroscience, Stanford Human Intracranial Cognitive Electrophysiology Program, Department of Neurology and Neurological Sciences, Stanford University, Stanford, CA 94305, USA

[3]These authors contributed equally

[4]Senior author

[5]Lead contact

SUMMARY

Hippocampal ripples are prominent synchronization events generated by hippocampal neuronal assemblies. To date, ripples have been primarily associated with navigational memory in rodents and shortterm episodic recollections in humans. Here, we uncover different profiles of ripple activity in the human hippocampus during the retrieval of recent and remote autobiographical events and semantic facts. We found that the ripple rate increased significantly before reported recall compared to control conditions. Patterns of ripple activity across multiple hippocampal sites demonstrated remarkable specificity for memory type. Intriguingly, these ripple patterns revealed a semantization dimension, in which patterns associated with autobiographical contents become similar to those of semantic memory as a function of memory age. Finally, widely distributed sites across the neocortex exhibited ripple-coupled activations during recollection, with the strongest activation found within the default mode network. Our results thus reveal a key role for hippocampal ripples in orchestrating hippocampal-cortical communication across large-scale networks involved in conscious recollection.

In brief

Norman et al. report that synchronous hippocampal bursts (ripples) selectively emerge when patients recall past autobiographical events. Those ripples form spatial patterns that become

*Correspondence: itzik.norman@gmail.com (Y.N.), rafi.malach@gmail.com (R.M.).

AUTHOR CONTRIBUTIONS

Y.N. and O.R. conceived the study. J.P. designed the experiment. Y.N. analyzed the data. R.M. supervised the analysis. J.P. supervised the experiments and all aspects of data collection. O.R. contributed to data curation and analysis of behavioral data and assisted in writing several sections in the text. S.L. contributed to the detection of pathological high-frequency oscillations (HFOs). Y.N. and R.M. wrote the paper. J.P. and O.R. further contributed to the writing by reviewing and editing the manuscript.

SUPPLEMENTAL INFORMATION

Supplemental information can be found online at https://doi.org/10.1016/j.neuron.2021.06.020.

DECLARATION OF INTERESTS

The authors declare no competing interests.

increasingly similar to semantic-memory patterns, the more remote the memory. The results demonstrate the pivotal role of ripples in coordinating recollections in the human brain.

INTRODUCTION

The neuronal mechanisms that endow the human brain with its ability to flexibly retrieve and reexperience personal events (hereafter, autobiographical memory, or “autobio”) are still far from being understood. In recent years, a growing body of research, conducted primarily in rodents (Buzsáki, 2015) but also in non-human primates (Leonard and Hoffman, 2017; Logothetis et al., 2012), has focused on particularly robust neuronal synchronization events called sharp wave ripples (SWRs). Extant evidence from animal studies suggests a role for SWRs in the reactivation of mnemonic information (Davidson et al., 2009; Karlsson and Frank, 2009; Peyrache et al., 2009; Shin et al., 2019; Takahashi, 2015; Wu et al., 2017) and offline consolidation of rodents’ spatial (Ego-Stengel and Wilson, 2010; Fernández-Ruiz et al., 2019; Girardeau et al., 2009; Jadhav et al., 2012; Maingret et al., 2016; van de Ven et al., 2016), emotional (Girardeau et al., 2017; Gomperts et al., 2015), and social memories (Oliva et al., 2020).

Human memory research, beginning with the seminal work of Scoville and Milner (1957) and others (Kartsounis et al., 1995; Rosenbaum et al., 2000; Vargha-Khadem et al., 1997), primarily emphasized the role of the hippocampus in the encoding and retrieval of autobiographical memory (Barry and Maguire, 2019; Elward et al., 2021; Gilboa et al., 2004; Maguire, 2001; Moscovitch et al., 2005; Nadel and Moscovitch, 1997; Ryan et al., 2001; Tulving, 2002), as well as in other forms of long-term declarative memory (Squire and Zola, 1996; Squire et al., 2004). The contribution of hippocampal ripples to the dynamics of human declarative memory processes is still unknown. More generally, little is known about the relationship between hippocampal ripples and the intrinsic mental contents that emerge in the conscious mind of an individual.

In the present work, we took advantage of rare multisite intracranial electroencephalographic (iEEG) recordings (Parvizi and Kastner, 2018) obtained directly from the hippocampus and cerebral cortex of neurosurgical epileptic patients. Using this approach, it is possible to reliably detect and study hippocampal ripples in the human brain (Axmacher et al., 2008; Helfrich et al., 2019; Norman et al., 2019; Staresina et al., 2015; Vaz et al., 2019, 2020; Zhang et al., 2018). In prior work, ripples were implicated in the awake retrieval of recently acquired visual memories (Norman et al., 2019), word-pair associations (Vaz et al., 2019, 2020) and face-profession associations (Henin et al., 2021). However, the question of whether and in what manner hippocampal ripples support the retrieval of longer-term declarative memories in the human brain remains unknown.

Another important issue that is still unresolved concerns the role of ripples in establishing a cortical-hippocampal communication during conscious recollection. In particular, a large number of human brain studies have implicated a specific cortical network, the default mode network (DMN), as playing a central role in episodic memory (Buckner and Carroll, 2007; Fox et al., 2018; Harmelech et al., 2015; Raichle, 2015; Schacter et al., 2012). A major advantage of intracranial recordings in patients is the ability to simultaneously

record hippocampal ripples and cortical responses while the patients are engaged in various cognitive tasks. Here, we leveraged this methodology to directly study the ripple-triggered hippocampal-cortical interplay during long-term autobiographical and semantic memory recall.

RESULTS

Experimental design and intracranial recordings

The study was based on recordings obtained in 20 patients (10 females) with refractory epilepsy implanted with intracranial electrodes in the hippocampus and various cortical sites as part of their neurosurgical evaluation at Stanford University Medical Center. Hippocampal ripples were identified using a modification of our previously described procedure (Norman et al., 2019) (see STAR Methods).

The experimental design is depicted in Figures 1A-1C. In short, patients were asked to make true/false judgments about a series of visually presented statements. These statements required the retrieval of autobiographical memories of varying degrees of remoteness (i.e., events that happened today, yesterday, 1 week ago, or last month) or of semantic facts (in 11 patients). In a control condition, patients were asked to solve arithmetic problems (see summary of behavioral performance in Table S1).

An example of the multicontact electrodes that were implanted in the hippocampus is depicted in Figures 1D and 1E (see Table S3 for details). Hippocampal ripples were identified by their relatively transient, high-frequency profile (Figures 1F-1H; see also STAR Methods). An overview of ripple rates (throughout the entire experiment) for the 112 hippocampal sites included in our analysis is depicted in Figure 1I.

Elevated ripple rate during autobiographical memory retrieval

To determine whether hippocampal ripples are associated with conscious memory retrieval processes, we examined the ripple rate during different conditions. This revealed a clear selectivity for autobiographical recall relative to arithmetic processing and awake rest. The ripple rate was computed individually in each recording site, from stimulus onset to reaction time (RT), and was averaged across all sites within a patient (see Figure 2A, sign-rank test, autobio versus rest: $p = 0.0072$; autobio versus math: $p = 0.0002$, math versus rest: $p = 0.0028$; $n = 20$ patients). Examining the dynamic evolution of ripple rates during the task (Figures 2C and 2D) revealed a striking discrepancy between the autobio and math conditions, with the latter notably showing suppressed responses compared to a 5-s cued rest condition ($p < 0.01$, cluster-based permutation test; $n = 20$ patients). Ripple rates returned to baseline levels immediately after the patient's button-press response (Figure 2D). Similar results were found when examining a single representative contact in each patient (i.e., the closest contact to CA1; see Figures S2A-S2C).

Figure 2B depicts the distribution of the autobio versus math effect size across individual sites. Mixed-effect regression model fitted to the data (STAR Methods) revealed a significant link between autobio preference and electrode distance from CA1 ($F(1,82.90) = 19.38$, $p < 3.17 \times 10^{-5}$), brain hemisphere ($F(1,93.01) = 10.17$, $p = 0.0019$), and interaction between

hemisphere and hippocampal longitudinal position ($F(1,83.68) = 5.30$, $p = 0.023$) (see Figures 2E and 2F). Thus, preference to autobio trials was maximal in the left anterior hippocampus, increased with proximity to CA1, and was weakest in the right posterior hippocampus.

The autobiographical items recalled during the task were of varying degrees of remoteness (i.e., memories from today, yesterday, this week, or last month). This enabled us to examine whether memory age affected the overall ripple rate elicited during the autobiographical trials. To that end, we ran a mixed effects ANOVA (using a fixed factor for memory age and a random factor for electrode nested within patient; see STAR Methods). For consistency across conditions, ripple rates were computed in a fixed, generic time window of 2 s centered on the peak of the grand-average autobio response shown in Figure 2D (where ripple rate modulation was strongest). The results revealed a significant effect of memory age on the average ripple rate ($F(3,288) = 18.27$, $p < 10^{-10}$; n = 16 patients [4 patients were excluded from this analysis for not having the “last-month” condition]). Post hoc comparisons indicated that the ripple rate was higher during the retrieval of remote experiences compared to more recent memories (false discovery rate [FDR]-adjusted p values are reported in the figure). Complementary analyses of the ripple activation profile across the different levels of remoteness are depicted in Figures S2F and S2G.

Ripple activation profiles vary with retrieval difficulty

To examine whether ripple activation profiles varied depending on the difficulty of the retrieval process, we pooled together autobio trials across all patients (n = 1,475 trials) and sorted them by RT, taken here as a proxy for retrieval difficulty. For the analysis, we split the trials into 5 groups based on their RT quintile. We discarded the fastest and slowest trials in the 2 extremes (first and last RT quintiles, respectively) and remained with 3 groups: fast (n = 267), medium (n = 292), and slow (n = 286) trials (2^{nd}, 3^{rd}, and 4^{th} quintiles, respectively). We then computed ripples peri-event time histogram (PETH) aligned to the patients’ response separately for each trial group. Figures S2D and S2E depict the results of this analysis. We found that ripple activation during recall lasted longer and generated more ripples during slow compared to fast trials (see Figure S2E for details), suggesting that hippocampal ripple activation during retrieval is not an isolated response locked to the moment of actual recollection, but reflects pre-recall retrieval attempts as well.

Given this relationship with RT, it could be argued that the link between ripple rate and memory age reported above (Figure 2G) may in fact be a consequence of RT differences between recent and remote memories (since the latter may require a more extensive memory search). Examining the patients’ behavior revealed that RTs increased significantly with remoteness level (Figure S2H; $p = 0.005$, Friedman test, n = 16 patients; last month versus today: $p = 0.003$, signed-rank test). However, to examine whether such RT differences could account for the enhancement in ripple rate during retrieval (Figure 2G), we ran a control analysis in which we equated the RTs among the different levels of remoteness (see Figure S2 for details) and found that memory age still had a significant effect on ripple rate above and beyond the influence of RT.

Individual hippocampal ripples are spatially confined

To further characterize the nature of ripple rate modulation and to explore how local was the emergence of individual ripples across the hippocampus, we carried out the following analyses. First, we computed the trial-to-trial ripple rate correlations between neighboring electrode pairs (within a patient). This analysis revealed a significant correlation that quickly diminished as a function of inter-electrode distance (Figures S3A and S3B). Thus, pairs of electrodes farther than 10 mm apart, or electrodes on opposite hemispheres, showed a weak or no correlation with each other. Intriguingly, this pairwise correlation became more widespread during the cued rest condition (Figure S3B).

Second, we quantified the extent to which neighboring electrodes exhibited coincident activation of individual ripples. To that end, we computed the cross-correlogram of ripple events generated during autobio trials, separately for each pair of electrodes, and grouped the results by the level of inter-electrode distance (Figure S3C). Furthermore, we calculated for each electrode pair the proportion of coincident ripple activation (i.e., zero-lag events) out of the total number of ripples detected. Our results showed a significant but minor prevalence of ripple coincidences between adjacent electrodes of <4% ± 0.3% of the total number of ripples detected ($p < 0.01$, compared to chance level; see Figure S3D). Similar to the ripple rate correlations reported above, the proportion of ripples appearing simultaneously at different sites decreased sharply as a function of inter-electrode distance. These results highlight the local nature of ripple activation within the hippocampus, which is also consistent with observations in rodents (Patel et al., 2013).

Spatial patterns of ripples differentiate between memory types

To explore whether hippocampal ripple activity was biased toward specific types of declarative memory, we compared the average ripple rate across hippocampal sites in a subgroup of 11 patients who performed both the semantic and the autobiographical conditions. Interestingly, ripple activity during the semantic condition was of a magnitude similar to that of the autobiographical condition ($t(14.51) = 0.17$, $p > 0.87$, partially overlapping samples t tests (Derrick et al., 2017; see Figure 3A for details). For a comparison between the ripple activation profiles in each condition, see Figures S4A and S4B.

To examine whether there was functional specialization in individual recording sites for a specific memory type, we plotted the distribution of memory-type preference (effect size of autobio versus semantic trials) across all of the hippocampal sites. The obtained map pointed to a mosaic organization of memory-type biases (Figure 3B). Thus, ripple engagement during the two memory conditions appeared to be close to normally distributed, in a mixed and balanced manner across the two hippocampi. It should be noted, however, that a more fine-grained analysis using a mixed-effects model (similar to the one reported in Figure 2E) indicated that preference to semantic memory was slightly stronger in electrodes closer to the CA2/3 subfields, with no additional effects ($F(1,54.46) = 8.24$, $p = 0.0058$; see STAR Methods for further details).

Could memory type be coded in the patterns of ripple activations across multiple hippocampal sites, rather than the mean overall rate? To examine this possibility, we trained a linear discriminant analysis (LDA) classifier on the multivariate ripple-rate patterns emerging across conditions (STAR Methods). The LDA classifier was able to decode trial type (i.e., autobiographical, semantic, and math conditions) with significant accuracy ($p < 0.001$, Monte Carlo permutation test, shuffling condition labels 1,000 times; see Figure 3C). A confusion matrix analysis (Figure 3D) confirmed this observation and revealed higher confusion within memory types compared to the math condition. Notably, training and testing the classifier on memory trials alone, leaving math trials out of the analysis, revealed a similar result (Figure S4E).

Ripple pattern similarity reflects memory semantization

Next, having established that multisite ripple rate patterns are informative about memory content (autobio versus semantic), we addressed the intriguing question of whether the degree of similarity between ripple rate patterns associated with individual memory items could reflect natural processes of memory semantization, namely, the gradual transformation of autobiographical (episodic memory) representations into a format that is more akin to semantic memory. To examine this question, we grouped the recalled memory items by their age (i.e., degree of remoteness), starting from very recent autobiographical memories from today or yesterday, to more remote experiences from last week or last month, and calculated the similarity between the average ripple rate pattern in each group and the average pattern that emerged during semantic retrieval.

Strikingly, we found that ripple rate patterns associated with autobiographical memories gradually became similar to semantic memory as a function of memory age (Figure 4A). Thus, the more remote the autobiographical content was (e.g., “last month” versus “yesterday”) the more similar its associated ripple rate pattern was to the pattern of semantic memory (Figure 4A; see STAR Methods). This increase in pattern similarity cannot be explained solely on the basis of (univariate) differences in average ripple rate between conditions (Figure S4C). However, we do not rule out the possibility that such overall differences may have contributed to the result as well.

To statistically test the relationship between memory age and the distance from the semantic memory ripple rate pattern, we moved to the single-item level and computed the pattern dissimilarity distances (1-R) of each individual item from the average semantic memory pattern. We then placed these distances on an ordinal scale representing memory age: from “today” (the most recent memories), through “yesterday,” “this week,” and “last month” up to semantic memory (the most remote memories) and computed the Spearman’s correlation between these individual item distances and their respective memory age. The result indicated a highly significant negative correlation ($\rho = -0.47$, $p < 10^{-7}$, $n = 115$ items; Figure 4B).

Finally, agglomerative hierarchical clustering (using group-average linkage) applied to the average ripple rate patterns associated with each class of items revealed a similar result, with ripple rate patterns forming a hierarchy that reflects the episodic-semantic continuum.

Enhanced ripple rate linked to autobiographical statements judged as “TRUE”

To further characterize the relationship between ripple rate and the behavioral retrieval process, we compared ripple activity between autobio trials that ended up with the patient confirming the autobiographical statement (i.e., responded “TRUE”), and trials that ended up with the patient disaffirming the statement (i.e., responded “FALSE”). To that end, we computed the ripple rate during TRUE and FALSE autobio trials using a generic time window of 2 s centered on the peak of the grand-average autobio response. We found that a TRUE response elicited a significantly higher ripple rate compared to a FALSE response ($p = 0.002$, $n = 20$ patients, signed-rank test; Figure S4F). To make sure this effect was not due to a general bias to affirmatory answers, we conducted a similar analysis on semantic trials. The results indicated no difference between TRUE and FALSE responses during semantic trials ($p = 0.28$, $n = 11$ patients, signed-rank test; Figure S4G; incorrect trials (13.9%) were excluded from this analysis). This finding suggests that a TRUE autobio response engages a stronger retrieval process, perhaps due to richer and more specific memory associations.

Ripple-triggered cortical-hippocampal dialogue

As mentioned above, the iEEG method enabled us to simultaneously record from multiple cortical and hippocampal sites. Thus, we sought to examine the dynamics of cortical activations coupled to hippocampal ripple events. To disentangle the ripple-coupled cortical activations from those driven by the appearance of memory statements on the computer screen or subject’s button presses, we used a linear deconvolution analysis (Ehinger and Dimigen, 2019; Golan et al., 2016) (see STAR Methods). In this approach, the continuous high-frequency broadband (HFB; 60–160 Hz, also known as high gamma) time series in each cortical recording site is understood as a linear convolution of isolated neuronal responses with different experimental events (in our case, stimulus onset, hippocampal ripples, and button presses). By implementing a general linear model (GLM) in which the latencies of experimental events (and a number of time points around them) are added as predictors, we were able to isolate and recover the profiles of cortical HFB responses associated with each type of event, while accounting for the contributions of all of the other events simultaneously.

Figure 5A shows a schematic depiction of the GLM design matrix implemented in our analysis. Figure 5B presents an example of deconvolved HFB responses from two representative cortical sites in a single patient, which responded robustly to the autobio statements. In addition to the clear activation following stimulus presentation (center panels), the two electrodes exhibited a smaller but robust HFB activation coupled to the hippocampal ripple event (bottom panels).

How ubiquitous was the peri-ripple response across the cortex during the autobiographical retrieval condition? By integrating electrodes from all of the patients (830 bipolar cortical recordings in total), we were able to examine the spatial distribution of peri-ripple responses widely across the cortex. Figure 5C maps all of the cortical sites that exhibited a robust peri-ripple HFB response during the autobiographical retrieval condition. HFB amplitude was averaged over a time window of −250 to 250 ms relative to the hippocampal ripple event. The resulting map revealed a strikingly widespread yet anatomically consistent

distribution of peri-ripple activations (with very few examples of deactivation). Importantly, based on a cortical atlas of seven canonical resting-state networks (Yeo et al., 2011), we found a clear predilection of cortical structures within the DMN (pink-colored regions), which we show quantitatively in Figure 5D (top left panel). Notably, peri-ripple activation in DMN electrodes was significantly stronger compared to the other networks ($p < 0.05$, FDR-corrected rank-sum tests). See Figure S6A for a comparison between DMN and non-DMN sites within subjects. Importantly, alongside the DMN, sites within the limbic network also showed considerable peri-ripple activation, which is intriguing given their link to depression, rumination, and maladaptive retrieval of autobiographical contents (Hamilton et al., 2015).

Peri-ripple cortical activation profile

Next, we investigated the temporal relationship of the peri-ripple cortical responses to the timing of the hippocampal ripple events. Analysis of the peri-ripple dynamics across the main resting-state cortical networks showed that the peri-ripple activations were generally centered on the hippocampal ripple peak (Figure 5D).

Similar activation profiles were obtained when sampling cortical areas based on purely anatomical definitions (i.e., using a gyral-based atlas; Figure S5A). Examining potential asymmetries in the peri-ripple responses relative to the peak of the ripple revealed dynamics that varied over a continuum, with some anatomical areas showing a slight bias toward leading the hippocampal ripple and others showing a slight bias toward trailing the ripple (Figures S5B and S5C). Notably, this result is in line with a recent report in rodents (Karimi Abadchi et al., 2020).

Were the peri-ripple responses stronger in cortical sites that demonstrated memory selectivity—that is, sites that showed stronger stimulus response to autobio statements compared to math (see STAR Methods)? Comparing across all task-responsive cortical electrodes supported this bias (Figure 6A). We found a significant correlation between memory selectivity (computed on the first run) and peri-ripple response magnitude (computed on the second run) both for the entire cortex (right; Spearman's $\rho = 0.3$, $p < 10^{-11}$) and the DMN in isolation (left; Spearman's $\rho = 0.44$, $p < 10^{-4}$).

Focusing specifically on cortical sites that showed significant memory selectivity ($p < 0.05$ FDR adjusted, autobio versus math; see Figure 6B for anatomical location and left panel in Figure 6C for deconvolved stimulus response), we found significantly stronger peri-ripple responses during memory retrieval compared to both the cued 5-s rest and the math condition ($p < 0.001$, cluster-based permutation test; Figure 6C, right panel). Intriguingly, comparing the peri-ripple responses across semantic and autobio conditions revealed similar levels of activation (Figure S6G). For further comparison, analyzing a similar ensemble of "math-selective" cortical sites revealed a substantially weaker peri-ripple response during both autobio and math trials (Figures S6C-S6E).

The peri-ripple activation profile in individual memory-selective sites was comparable across DMN and non-DMN sites (Figure S6B), suggesting that the peri-ripple activation during recall is not specific to the DMN, but rather extends to other sites involved in memory processing. Estimating the latency of the peri-ripple activation peak using a

bootstrap sampling procedure suggested that the latency of peak activation during autobio and rest conditions was not significantly different from zero (peak latencies: autobio, 56 ± 72 ms; 5 s rest, 64 ± 73 ms; p = not significant [NS]). During math, however, peri-ripple activity was slightly delayed and peaked 96 ± 28 ms after the hippocampal ripple event ($p < 0.05$; see Figure S6F).

Lastly, to further validate the linear deconvolution approach, we carried out an independent analysis of memory-selective sites, in which the HFB time series were simply averaged relative to the latencies of hippocampal ripples (i.e., ripple-triggered averaging without deconvolution). Importantly, we compared the averages using the actual ripple latencies with the averages derived following shuffling of ripple latencies across trials (Figure S6H). Note that this shuffling procedure preserves the overall distribution of hippocampal ripple latencies with respect to the stimulus onset but eliminates the direct temporal link between the ripple and cortical activity within a trial. Subtracting the two averages allowed us to isolate the contribution of the actual temporal coupling between cortical HFB and hippocampal ripples. Reassuringly, the derived peri-ripple activation was strikingly similar to the one obtained from the deconvolution approach (Figure S6I).

DISCUSSION

Hippocampal ripples and long-term memory retrieval

Here, we reveal a direct link between the traditionally defined role of the human hippocampus as critical for long-term autobiographical memory (Moscovitch et al., 2016; Nadel and Moscovitch, 1997) and hippocampal ripples whose memory functions have typically been studied in the context of spatial navigation in rodents. Our study demonstrates the robust engagement of hippocampal ripples during human autobiographical retrieval. We also demonstrate a significant ripple activation during the retrieval of semantic facts, thus revealing an important mechanistic link between these two types of declarative memory (Renoult et al., 2019; Tulving and Markowitsch, 1998).

More specifically, we find a significant increase in ripple rates during the retrieval of long-term autobiographical memories of varying degrees of remoteness, as well as more abstract semantic knowledge. This effect could not be attributed to general cognitive effort or to decision making since solving math problems actually caused a reduction (below fixation baseline) in ripple rates (Figure 2D). Although hippocampal ripples are produced at a notoriously slow rate (~0.4 events/s), they showed a surprisingly tight temporal coupling to task performance, particularly to the termination of the memory recall process as indicated by the button presses (Figure 2D).

Interestingly, our results reveal a link between ripple activation profiles and RT (taken here as a proxy for retrieval difficulty). Across autobio trials, ripple rate enhancement was significantly extended during slow trials (i.e., memory statements that took patients longer to judge; Figures S2D and S2E), which suggests a role for hippocampal ripples, not only in the final moment of successful recall but also during more initial retrieval attempts. It should be noted that in the present task design, it was not possible to verify the correctness of the retrieved autobiographical memories.

The observation that remote memories elicit higher ripple rates compared to more recent memories (Figure 2G) may be taken as more evidence for a possible relationship between ripple rate and retrieval difficulty. However, interestingly, equating RTs among the different levels of remoteness indicated that memory age has an independent effect on ripple rate above and beyond RT differences.

Our study, which consisted of tens of hippocampal recording sites across a cohort of 20 neurosurgical patients, uncovered clear anatomical specializations with a stronger preference for autobiographical recall the closer the electrodes were to CA1, and in electrodes located in the left anterior hippocampus (Figures 2E and 2F). In addition to corroborating recent studies in rodents demonstrating a critical role for CA1 ripples in awake memory processes (Fernández-Ruiz et al., 2019; Jadhav et al., 2012; Joo and Frank, 2018; Shin et al., 2019), our findings are compatible with a human lesion study indicating a role for CA1 in autobiographical recall (Bartsch et al., 2011), as well as with fMRI (Gilboa et al., 2004; Maguire, 2001; Maguire and Frith, 2003; Viard et al., 2007) and neuropsychological (Barr et al., 1990) studies, showing that autobiographical memory retrieval is primarily lateralized to the left hippocampus. Interestingly, our results revealed preferential ripple activation in the anterior hippocampus. This may be compatible with the gist-like recollection strategy proposed to be represented in the anterior hippocampus (Sekeres et al., 2018).

Multisite patterns of ripple activation uncover a semantization process

While the overall ripple rate computed across all of the electrodes failed to reveal a clear differentiation between autobiographical and semantic memories (Figures 3A, S4A, and S4B), at the individual contact level, we did find discernible biases toward specific memory types (Figure 3B). This suggests that significant content information may reside in the multicontact ripple activation patterns rather than the overall ripple rate average. Multivariate pattern analysis succeeded in a significant decoding of memory type (autobio versus semantic). Remarkably, dissecting the memory content further by temporal remoteness of the recalled items (experiences from today to last month as well as longer-term semantic knowledge) revealed an intriguing dimension of semantization: a gradually increasing similarity between the ripple rate patterns associated with autobiographical memory and the average pattern associated with semantic memory, as autobiographical contents become more remote (Figures 4A-4C). This finding highlights collective multisite coding by ripples as an important aspect of hippocampal function. It raises the exciting possibility of ripple-based representational space in the hippocampus expressing processes of maturation, abstraction, and semantization of memories (Dudai et al., 2015; Nadel and Moscovitch, 1997; Renoult et al., 2019; Winocur and Moscovitch, 2011), encoded by the similarity distances of multisite ripple activation patterns. However, it is important to emphasize that at this stage, it is unclear what precise factor (e.g., memory remoteness) may have contributed to the observed semantization phenomenon.

It is important to note that hippocampal ripples represent a striking case of neuronal population coding rather than single neuron tuning. It is thus of interest to consider what could be the relationship of such population-level representation to single neuron properties shown to be linked to abstract concepts and various mnemonic processes (Gelbard-Sagiv

et al., 2008; Quiroga, 2012, 2019; Quiroga et al., 2005; Rutishauser et al., 2021; Staresina et al., 2019). Some hints can be derived from detailed rodent SWR studies showing a compressed replay of place sequences (Davidson et al., 2009; Diba and Buzsáki, 2007; Foster and Wilson, 2006). It is tempting to speculate based on this analogy that human hippocampal ripples represent rapid sequencing of concepts associated with the recalled memory content.

Implications for existing models of memory consolidation and transformation

Our results, showing enhanced ripple activity during remote compared to recent memory retrieval (see Figure 2) may have some relevance to a central debate concerning models of systems memory consolidation. In particular, they appear to support theories that emphasize richer hippocampal representations of remote memories (e.g., the multiple trace theory) (Nadel and Moscovitch, 1997) rather than a growing disengagement of the hippocampus with memory age (McClelland et al., 1995; Squire et al., 2015), at least as reflected in ripple rates. However, it should be noted that the involvement of ripples in remote retrieval does not rule out the possibility that remote memories, properly consolidated and incorporated in neocortical networks, may still be retrieved independently of the hippocampus, albeit in a less detailed format and with fewer contextual features (O'Reilly et al., 2014; Sekeres et al., 2018; Winocur and Moscovitch, 2011).

Role of ripples in the cortical-hippocampal interplay

A major hypothetical role attributed to ripples is coordinating hippocampal-cortical communication (Karimi Abadchi et al., 2020; Logothetis et al., 2012; Rothschild et al., 2017; Todorova and Zugaro, 2020). Our group and others have recently demonstrated that cortical activity is linked to hippocampal ripple events in the human brain (Helfrich et al., 2019; Ngo et al., 2020; Norman et al., 2019; Vaz et al., 2019, 2020; Zhang et al., 2018).

In the present study, we had the unique opportunity to examine the link between hippocampal ripples and cortical activations during long-term autobiographical recall. We used deconvolution analysis to disentangle the cortical peri-ripple responses (see Figure 5A and STAR Methods) and verified this procedure using a shuffling approach (Figures S6H and S6I). Data-driven examination of the distribution of cortical sites that showed a ripple-mediated hippocampal-cortical link during the autobiographical condition revealed a widespread distribution involving major cortical networks and sites (Figures 5C and 5D). Significantly, the DMN most prominently displayed an interaction with hippocampal ripples. This observation is compatible with recent reports in rodents (Karimi Abadchi et al., 2020), non-human primates (Kaplan et al., 2016), and human magnetoencephalography (Higgins et al., 2021). Moreover, our results are in line with recent iEEG studies in the human DMN (Fox et al., 2018) and a large body of fMRI studies (Buckner and Carroll, 2007; Harmelech et al., 2015; Kim, 2010; Schacter et al., 2012; Vatansever et al., 2021) demonstrating the role of DMN in autobiographical memory. The finding of peri-ripple responses in networks other than the DMN (albeit less pronounced) is compatible with the proposal that ripples play a coordinating role, not only in the reenactment of diverse multisensory representations (Fernández-Ruiz et al., 2019; Norman et al., 2019; Rothschild et al., 2017; Vaz et al., 2020; Zhang et al., 2018) but also in reactivating contextual information (Peyrache et al.,

2009; Takahashi, 2015), previous decisions (Shin et al., 2019), emotions (Girardeau et al., 2017; Gomperts et al., 2015; Wu et al., 2017), and other types of high-order representations (Todorova and Zugaro, 2020). Future studies are needed to highlight the precise interplay among DMN, limbic, and frontoparietal networks during, for example, rumination and reappraisal of memories.

Theoretical models (Robin and Moscovitch, 2017; Sekeres et al., 2018) and recent neuroimaging studies in humans (McCormick et al., 2018, 2020) suggest that the ventromedial prefrontal cortex, mainly via interactions with the anterior hippocampus, represents common aspects across events (i.e., abstract schema-like representations). Our results provide further details related to these cortical hippocampal interactions.

Thus, examining the dynamics of the cortical activation with respect to the hippocampal ripple event, we found that peri-ripple cortical responses varied over a continuum of anticipatory and trailing-biased activations (Figure S5). This finding is compatible with our previous observations in the case of visual recall (Norman et al., 2019) as well as findings in rodents (Karimi Abadchi et al., 2020; Rothschild et al., 2017; Todorova and Zugaro, 2020). These dynamics are consistent with a recurrent interplay between the cortex and hippocampus, in which the cortex participates in seeding hippocampal representational content before the ripples and, in turn, is amplified by these ripple events (Rajasethupathy et al., 2015; Rothschild et al., 2017). This process likely enables the coordination and integration of mnemonic information across large-scale brain networks involved in memory recall (Karimi Abadchi et al., 2020; Rothschild et al., 2017).

Conclusions

Our results both confirm and extend previous demonstrations of hippocampal ripples in human conscious recollection (Henin et al., 2021; Norman et al., 2019; Vaz et al., 2019, 2020). First, they demonstrate that the hippocampal ripples are tightly involved in the retrieval of personal autobiographical memories, while being downregulated during non-memory-based cognitive processes. Second, they link ripples to both recent and remote recollections and to semantic memory. Third, they highlight a new coding scheme of ripples based on multisite ripple activation patterns. Finally, they reveal a complex and extensive hippocampal-cortical dialogue that emerges during recollection and includes distributed ripple-coupled activations in the DMN as well as in a variety of other cortical sites.

STAR★METHODS

RESOURCE AVAILABILITY

Lead contact—Further information and requests for resources should be directed to Y.N. (itzik.norman@gmail.com).

Materials availability—This study did not generate any new reagents.

Data and code availability—Raw data and analysis code that support the conclusions of this study are available for public download on Zenodo: https://doi.org/10.5281/zenodo.4759103.

EXPERIMENTAL MODEL AND SUBJECT DETAILS

Participants—20 patients (10 females; demographics and electrode coverage information are included in Tables S2 and S4) with medicine-resistant epilepsy were implanted with intracranial depth electrodes (Ad-Tech Medical Instruments) as part of their pre-surgical evaluation at Stanford University Medical Central. The location of the implanted electrodes was determined by clinical evaluation for respective surgery. The current cohort was chosen on the basis of electrode coverage in the hippocampus (right or left) and participation in at minimum two blocks of the task. Each patient was monitored in the hospital for ~6-10 days and provided written informed consent to participate in the study, which was approved by the Stanford Institutional Review Board.

METHOD DETAILS

Intracranial EEG recordings—All electrophysiological data were recorded using a Nihon Kohen clinical monitoring system with a sampling rate of ≥ 1000 Hz and a band pass filter of 1.6-300Hz. The diameter of depth electrodes was commonly 0.86 mm, height was 2.29 mm, and distance between the centers of two adjacent electrodes was 5 mm (see Table S3 for precise electrode dimensions in each patient).

Electrode anatomical localization—Imaging data were acquired using a GE Healthcare 3 tesla SIGNA scanner at Stanford University equipped with a head coil. A T1-weighted SPGR pulse sequence was aligned along the anterior commissure-posterior commissure and was resampled at 1mm isotropic voxels, then segmented to distinguish gray and white matter using Freesurfer v6.0.0 (Fischl, 2012). For each subject, the postimplant CT scan was co-registered to the preimplant MRI anatomical scan using the iELVis toolbox (Groppe et al., 2017). We then manually labeled the electrode locations in BioImage Suite (Papademetris et al., 2006) and displayed them on the subject's own reconstructed 3D cortical surface. In the group-level analyses, we use iELVis to display all electrodes on a single cortical template (either "fsaverage" or "MNI305"). We used SUMA to resample and standardize the cortical template (Argall et al., 2006; Saad and Reynolds, 2012), which enabled us to display electrodes on a flattened cortical template while establishing node-to-node correspondence between meshes. Finally, each individual electrode was registered on two anatomical atlases: a gyral-based cortical atlas ("Desikan-Killiany") (Desikan et al., 2006) and a functional-connectivity-based atlas (Yeo et al., 2011). The latter allowed us to group cortical electrodes according to their anatomical affiliation to seven canonical "resting-state" networks. The assignment of atlas labels to electrodes was done in the native space of each brain. Electrodes farther than 3 mm from the cortical ribbon were excluded. Unless otherwise stated, when cortical recording sites (i.e., bipolar pairs) were grouped together based on their atlas label, it was sufficient that at least one of the electrodes that make up the bipole be located in the attributed region (which allowed for certain sites to be attributed to two different regions, when falling on the border between regions).

Experimental paradigm—The experiment was administered at patient clinical suite using Psychophysics Toolbox (Brainard, 1997) (http://psychtoolbox.org/) in MATLAB (The MathWorks) running on the Apple Macintosh OSX operating system. The laptop was positioned ~70cm from subjects' eyes at chest level. In the experiment, subjects were

instructed to make true or false judgements for a series of visually presented statements, requiring either autobiographical memory retrieval (e.g., “I went to the beach last month”), arithmetic processing (e.g., “42 + 11 =51”) or semantic knowledge (only in eleven subjects; e.g., “Babe Ruth was a football player”).

The memory statements that we used were generic and were not tailored according to the patient’s personal experiences or knowledge. Importantly, autobiographical memory statements concluded with words denoting the approximate time elapsed since the event in question, to allow an examination of four different levels of memory remoteness (18-20 items per each level): (1) “today/this morning” (e.g., I took my medicine *today*); (2) “yesterday/last night” (e.g., I had chicken for dinner *yesterday)*; (3) “this week” (e.g., I used my credit card this week); and (4) “last month” (e.g., I went to a wedding *last month*).

All statements were occasionally interspersed with fixation periods (5 s or 10 s) during which subjects were asked to fixate at a center crosshair (“cued 5s-rest” condition; for consistency we only used the first 5 s). A 500-ms period of blank screen separated trials (ITI).

All subjects completed two experimental runs, with a total of 73 autobiographical trials, 79 math trials and 37 semantic trials (in 11 subjects) on average (see Table S1 for more details). To reduce the likelihood that subjects relied on memorized addition tables, math equations always consisted of a two-digit number and a one-digit number.

Subjects respond to each statement by pressing one of two keypad buttons. The trials were terminated upon the subject’s button press or automatically after 15 s. Trial onset times were tagged using a photodiode for patients or an RTBox device (Li et al., 2010). In both cases, the tag was sent to an empty (DC) channel on the EEG montage and triggered within our task codes.

Preprocessing and data analysis—Data analysis was performed in MATLAB 2018b (MathWorks Inc., Natick, MA) using EEGLAB v14.1.2 (Delorme and Makeig, 2004), DRtoolbox (https://lvdmaaten.github.io/drtoolbox/), MES toolbox (Hentschke and Stüttgen, 2011), Unfold 1.1 EEG Deconvolution Toolbox (Ehinger and Dimigen, 2019), and custom-developed analysis code. The raw iEEG signal was inspected statistically to detect noisy/corrupted channels to exclude from further analyses. Specifically, channels whose voltage values, voltage derivative or RMS in the 99^{th} percentile were 5 SD greater than the rest of the electrodes were marked for exclusion after visual inspection in time and frequency domains. The preprocessing began by converting all healthy iEEG signals into bipolar derivations by pairing adjacent recording sites located on the same electrode probe. Recording sites in the hippocampus were paired with a nearby electrode contact located in white-matter, as identified anatomically using FreeSurfer’s segmentation (Fischl, 2012). We then notch-filtered the signal to remove 60 Hz power line interference (as well as its harmonics at 120Hz and 180 Hz) using a zero-lag linear-phase Hamming-windowed FIR band-stop filter (3 Hz wide).

High-frequency broadband signal—High-frequency broadband (HFB) signal (also known as high-gamma) was defined in the current study as the mean normalized power of frequencies between 60–160 Hz. Activity in this frequency range has been shown to be an excellent electrophysiological marker of local neuronal spiking activity (Mukamel et al., 2005; Parvizi and Kastner, 2018; Watson et al., 2018). HFB power was computed by filtering the signal in 20 Hz bands between 60-160 Hz (using zero-lag linear-phase Hamming-windowed FIR filters of order 138) and calculating the normalized, 1/f corrected, analytic amplitude using a Hilbert transform (Norman et al., 2017). To detect transient electrical artifacts that may interfere with the HFB signal, we also computed the HFB time-series of the common average signal (mean LFP across all non-corrupted monopolar iEEG channels) and detected peaks that exceeded 5σ. Time windows of 250 ms around these peaks were logged for exclusion in subsequent analyses.

Identification of memory/math selective sites—In the analysis of peri-ripple cortical activations we functionally defined two groups of electrodes based on their HFB evoked by the stimuli. First, based on previously observed late-onset activations for the current task in several cortical regions (Daitch and Parvizi, 2018; Foster et al., 2015; Raccah et al., 2018), we averaged the HFB amplitude over a generic time window of 300-2000 ms post-stimulus. Next, we pooled together all electrodes that exhibited some response to the main experimental conditions – i.e., autobiographical memory or math trials ($p < 0.05$ uncorrected, signed-rank test comparing the post-stimulus response to a pre-stimulus baseline). Finally, out of this general group of task-responsive electrodes we defined two subgroups of electrodes based on their selectivity to the autobiographical and math conditions. This was done by comparing the HFB response during the autobio condition to math (in the same generic time-window). Cortical electrodes that showed a significant preference to the autobiographical memory condition were regarded as ‘memory-selective’, whereas electrodes showing the opposite preference were regarded as ‘math-selective’ ($p < 0.05$, FDR adjusted, Wilcoxon rank-sum test comparing memory versus math; see Figures 6 and S6).

Hippocampal ripples detection—Ripple detection was performed on electrodes located within less than 2 mm from the hippocampal subfields CA1, CA2/CA3 and subiculum, i.e., the main hippocampal output stations, where sharp wave ripple events appear most prominently (Chrobak and Buzsáki, 1996; Oliva et al., 2016) (the exact anatomical locations of each recording site are depicted in Figure S1). Individual hippocampal subfields were delineated and reconstructed based on the patients’ pre-surgical MRI, using the parcellation algorithm included in FreeSurfer (Iglesias et al., 2015). Prior to ripple detection, a reference signal from a nearby white-matter contact was subtracted to eliminate common noise. The iEEG time series were then filtered between 70-180Hz (zero-lag linear-phase Hamming windowed FIR filter with a transition bandwidth of 5 Hz) and their instantaneous analytic amplitude was computed using a Hilbert transform. Based on our previously published procedure (Norman et al., 2019), extreme values were robustly estimated using Least-Median-Squares (LMS) (Seheult and Green, 1989) and clipped to 4 SD above the mean to minimize ripple-rate induced biasing. The clipped signal was then squared and smoothed (Kaiser-window FIR low-pass filter with 40 Hz cutoff), and the mean and SD

were computed across the entire experimental duration to define the threshold for event detection. Events from the original (squared but unclipped) signal that exceeded 4 SD above baseline were selected as candidate hippocampal ripple events. Event duration was expanded until ripple power fell below 2 SD. Events shorter than 20ms or longer than 200ms were excluded. Adjacent events with less than 30ms separation (peak-to-peak) were merged. Finally, ripple peak was aligned to the trough (of the non-rectified signal) closest to the peak ripple-band power.

A control detection was performed on the common average signal computed across all iEEG channels. Hippocampal ripple events that coincided with common average ripple-band peaks were removed, thus avoiding erroneous detection of transient electrical and muscular artifacts that tend to appear simultaneously on multiple channels (Fiederer et al., 2016).

To avoid inclusion of possible pathological events, we discarded any ripple that occurred within 100 ms from inter-ictal epileptic discharges (Gelinas et al., 2016) (IED). The latter were detected by filtering the raw hippocampal LFP between 25-60Hz (zero-lag linear-phase Hamming windowed FIR filter), and similar to the above procedure, rectifying, squaring, smoothing, normalizing and detecting events that exceeded 4 SD.

Importantly, hippocampal ripples were differentiated from pathological high-frequency oscillations (HFOs) that may appear in epileptic sites (Bragin et al., 2010). A supplementary analysis verified that the latter had no influence on the main results described above. Specifically, we evaluated how sensitive our results were to misidentification of physiological ripples with pathological High Frequency Oscillations (HFOs). We used our previously published technique (Liu and Parvizi, 2019; Liu et al., 2016) to identify HFOs in the hippocampus that demonstrated typical pathological attributes. We then discarded all ripples that occurred within 100 ms from the identified HFOs (on average: 5.5 ± 0.7% of the ripples detected in each electrode; 4 patients did not exhibit pathological HFOs at all) and re-run the main analyses. None of the main results showed a qualitative change following this procedure.

QUANTIFICATION AND STATISTICAL ANALYSIS

Peri-ripple spectrogram—Spectral decomposition of ripple events in hippocampal recording sites was done using a Morlet-wavelet time-frequency method, implemented in EEGLAB (Delorme and Makeig, 2004). We used a window of 1 cycle at the lowest frequency (4 Hz) and up to 20 cycles at the highest plotted frequency (250 Hz), with a step size of 4 ms. The spectrograms were then normalized by dividing the calculated power by the geometric mean power in each frequency (averaged over the entire peri-ripple epoch length [−750 to 750 ms] and across all epochs belonging to the same experimental run).

Multivariate pattern analysis of hippocampal ripple rates—Ripple rate patterns were constructed by pooling the hippocampal recording sites from the eleven patients that had both autobiographical and semantic conditions (patients that were presented with the exact same set of statements). To construct multivariate ripple-rate patterns associated with each item (statement), we first computed ripple rate per trial (number of ripples divided by trial duration from stimulus onset to reaction time in seconds), individually for

each recording site. We then applied z-score transformation across the different items and replaced any missing values by the mean of the corresponding trial group (in that recording site). Recording sites with more than 10% of items missing were excluded from the analysis. Similarly, items for which more than 10% of recording sites had a missing ripple rate value were excluded. This resulted in a matrix of 192 items × 65 hippocampal electrodes (Figure S4D, left panel).

We then centered the different patterns (matrix columns) around zero using z-score transformation, and applied a Principal Components Analysis (PCA) to reduce the dimensionality of the patterns using drtoolbox (https://lvdmaaten.github.io/drtoolbox/)(Van Der Maaten et al., 2009). Based on analysis of PCA eigenvalues, we required that each retained component would explain at least 2.5% of the variance. Using this criterion, we selected the top 11 principal components that collectively explained 42% of the variance (Figure S4D, right panel). Notably, including more principal components in the analysis did not change the main results.

To quantify the dissimilarity between condition-specific ripple activation patterns (math, semantic and autobiographical memories from today, yesterday, this week and last month;Figure 4) we conducted a bootstrap sampling procedure with 10,000 iterations to compute the mean and SE of the pairwise distances between the average pattern of each class of items. The distance between patterns was defined as 1-R (where R is the Pearson's correlation between the two patterns).

Pattern classification analysis—We trained a linear discriminant analysis (LDA) classifier using the MATLAB function *fitcdiscr.m* to decode trial type (autobiographical statements/semantic statements/math) from ripple rate patterns (constructed as detailed above). Classification performance was quantified using the F1-score (i.e., harmonic mean of precision and sensitivity) computed using a leave-one-out cross-validation technique. Statistical significance was determined by shuffling item labels 1,000 times and re-measuring classification performance in each iteration. P values were computed as the proportion of shuffled data F1-scores greater than or equal to the actual performance.

Deconvolution of peri-ripple cortical HFB activation—We used a time-domain deconvolution analysis to disentangle ripple-coupled cortical activity from other task-driven cortical responses. The analysis was implemented using the Unfold toolbox (Ehinger and Dimigen, 2019). See reference for a detailed mathematical description of the deconvolution procedure. In brief, the continuous HFB signal was down sampled to 250 Hz and entered into a multiple linear regression model. This model describes the observed time-series in each cortical site as the linear sum of overlapping (but separable) event-related HFB responses associated with the following experimental events: (i) stimulus onset; (ii) hippocampal ripples and (iii) button-press (i.e., reaction time). For consistency, ripple time-stamps in each patient were determined using a single hippocampal contact – the one that was closest to CA1 (those reported in Figures S2A-S2C). In this linear model, the design matrix coding the latencies of the events is expanded in time, so that each type of event is modeled by a set of predictors – in our case, 55 cubic splines basis-functions – spanning a time window of −1.5 to 4 s relative to event onset. Importantly, since these experimental

events occurred at different latencies throughout the experiment, it was possible to find a unique solution for the predictors' beta values that will best explain the measured HFB timeseries. This solution in fact isolates the unique contribution of each type of event in the overall HFB activity observed – taking into account the contribution of all event types simultaneously. These beta values are expressed in the same units of the original HFB time-series entered into the model; in our case, normalized HFB amplitude expressed in dB (10 × log10) relative to the mean amplitude during the 5 s rest (fixation) intervals. Notably, we computed the model twice, including either a single run of the task (Figure 6A) or both runs together (in all other analyses). In the group-level analysis shown in Figures 5 and 6 we excluded all recording sites that were located on the same depth electrode of the CA1 contact that contributed the time-stamps of the ripples. This was done to ensure that none of the peri-ripple cortical activations observed were due to a direct "leakage" of high-frequency electrical activity appearing on the hippocampal site.

Statistical tests—Statistical analyses were typically performed in MATLAB. Mixed effects analysis was performed in R (see dedicated section below). Pairwise comparisons were carried out using two-sided Wilcoxon signed-rank and rank-sum tests, unless stated otherwise. No statistical methods were used to predetermine sample sizes; however, sample sizes were similar to those generally employed in the field (Helfrich et al., 2019; Norman et al., 2019; Vaz et al., 2019). The unit of analysis was typically individual patients. In some cases, the unit of analysis was individual electrodes or patterns across ensembles of electrodes (see main text). Resampling tests were performed either using a custom-made MATLAB code or using previously published routines (Groppe et al., 2011) implemented in the Mass Univariate ERP Toolbox (OpenWetWare, 2015). Multiple comparisons correction was done using false discovery rate adjustment (FDR) (Benjamini and Yekutieli, 2001). When cluster-based permutation tests were implemented, family-wise error rate was inherently controlled in our method (Groppe et al., 2011; Maris and Oostenveld, 2007). Data collection was performed blind to the conditions of the experiment. Data analysis was not blind to the conditions of the experiments.

Mixed-effects analysis—Mixed-effects analyses were carried out using the LME4 package (Bates et al., 2015) implemented in R (R Core Development Team, 2017). Data were fitted with a random intercept model with the relevant fixed factors and a random factor of 'Patient' (or 'Electrode' nested within 'Patient'). The latter accounts for the fact that different participants contributed different numbers of electrodes to the analysis. In the analyses of autobio-versus-math preference (Figures 2E and 2F) and autobio-versus-semantic preference the models were formulated as follows:

$$\text{Hedges}'g \sim \text{CA1}_{\text{dist}} + \text{CA2,3}_{\text{dist}} + \text{Subiculum}_{\text{dist}} + \text{LongPosition} + \text{Hemisphere} + \text{LongPosition} \times \text{Hemisphere} + (1 \mid \text{Patient})$$

Where the terms representing distance from hippocampal subfields are continuous variables, and terms representing the hemisphere (left/right) or the longitudinal position (anterior/posterior) of the electrode are categorical variables with two levels each. In the analysis of

the trial-to-trial correlation between electrodes the model was formulated as follows (see Figure S3B for more details):

$$\text{Correlation} \sim \text{ElectrodeDistance} \times \text{Condition} + (1 \mid \text{Patient} / \text{ElectrodePair})$$

Finally, in analyses that examined the effect of memory age on ripple rates (Figures 2G and S4C), we included a single fixed factor representing the memory age category and a nested random factor of (Patient/Electrode), which accounted for the fact that different participant contributed a different number of electrodes to the analysis. The model was formulated as follows:

$$\text{Rate} \sim \text{MemoryAgeCategory} + (1 \mid \text{Patient} / \text{Electrode})$$

Main effects were tested using Type III ANOVA implemented in the afex R package (Singmann et al., 2020). Degrees of freedom were computed using the Kenward-Roger (KR) method. Post hoc comparisons were carried out using lsmeans R package (Lenth 2016) and were corrected for multiple comparisons using FDR (Benjamini and Yekutieli, 2001).

Supplementary Material

Refer to Web version on PubMed Central for supplementary material.

ACKNOWLEDGMENTS

We thank the patients who graciously volunteered to participate in the experiments; members of the Stanford Comprehensive Epilepsy Program; and members of the Laboratory of Behavioral and Cognitive Neuroscience, especially Claire Megan Perry, Clara Sava-Segal, and So Ri Baek, who assisted with recruiting patients and recording and transferring data. This work was supported by NIH grant no. R21NS113024 (to J.P.), a CIFAR Tanenbaum Fellowship (to RM.), and a National Science Foundation Graduate Research Fellowship (DGE 1839302) (to O.R.).

REFERENCES

Argall BD, Saad ZS, and Beauchamp MS (2006). Simplified intersubject averaging on the cortical surface using SUMA. Hum. Brain Mapp 27, 14–27. [PubMed: 16035046]

Axmacher N, Elger CE, and Fell J (2008). Ripples in the medial temporal lobe are relevant for human memory consolidation. Brain 131, 1806–1817. [PubMed: 18503077]

Barr WB, Goldberg E, Wasserstein J, and Novelly RA (1990). Retrograde amnesia following unilateral temporal lobectomy. Neuropsychologia 28, 243–255. [PubMed: 2325837]

Barry DN, and Maguire EA (2019). Remote Memory and the Hippocampus: A Constructive Critique. Trends Cogn. Sci 23, 128–142. [PubMed: 30528612]

Bartsch T, Döhring J, Rohr A, Jansen O, and Deuschl G (2011). CA1 neurons in the human hippocampus are critical for autobiographical memory, mental time travel, and autonoetic consciousness. Proc. Natl. Acad. Sci. USA 108, 17562–17567. [PubMed: 21987814]

Bates D, Mächler M, Bolker B, and Walker S (2015). Fitting Linear Mixed-Effects Models Using {lme4}. J. Stat. Softw 67, 1–48.

Benjamini Y, and Yekutieli D (2001). The control of the false discovery rate in multiple testing under dependency. Ann. Stat 29, 1165–1188.

Bragin A, Engel J Jr., and Staba RJ (2010). High-frequency oscillations in epileptic brain. Curr. Opin. Neurol 23, 151–156. [PubMed: 20160649]

Brainard DH (1997). The Psychophysics Toolbox. Spat. Vis 10, 433–436. [PubMed: 9176952]

Buckner RL, and Carroll DC (2007). Self-projection and the brain. Trends Cogn. Sci 11, 49–57. [PubMed: 17188554]

Buzsáki G (2015). Hippocampal sharp wave-ripple: a cognitive biomarker for episodic memory and planning. Hippocampus 25, 1073–1188. [PubMed: 26135716]

Chrobak JJ, and Buzsaki G (1996). High-frequency oscillations in the output networks of the hippocampal-entorhinal axis of the freely behaving rat. J. Neurosci 16, 3056–3066. [PubMed: 8622135]

Daitch AL, and Parvizi J (2018). Spatial and temporal heterogeneity of neural responses in human posteromedial cortex. Proc. Natl. Acad. Sci. USA 115, 4785–4790. [PubMed: 29666262]

Davidson TJ, Kloosterman F, and Wilson MA (2009). Hippocampal replay of extended experience. Neuron 63, 497–507. [PubMed: 19709631]

Delorme A, and Makeig S (2004). EEGLAB: an open source toolbox for analysis of single-trial EEG dynamics including independent component analysis. J. Neurosci. Methods 134, 9–21. [PubMed: 15102499]

Derrick B, Toher D, and White P (2017). How to compare the means of two samples that include paired observations and independent observations: a companion to Derrick, Russ, Toher and White (2017). Quant. Methods Psychol 13, 120–126.

Desikan RS, Ségonne F, Fischl B, Quinn BT, Dickerson BC, Blacker D, Buckner RL, Dale AM, Maguire RP, Hyman BT, et al. (2006). An automated labeling system for subdividing the human cerebral cortex on MRI scans into gyral based regions of interest. Neuroimage 31, 968–980. [PubMed: 16530430]

Diba K, and Buzsáki G (2007). Forward and reverse hippocampal place-cell sequences during ripples. Nat. Neurosci 10, 1241–1242. [PubMed: 17828259]

Dudai Y, Karni A, and Born J (2015). The Consolidation and Transformation of Memory. Neuron 88, 20–32. [PubMed: 26447570]

Ego-Stengel V, and Wilson MA (2010). Disruption of ripple-associated hippocampal activity during rest impairs spatial learning in the rat. Hippocampus 20, 1–10. [PubMed: 19816984]

Ehinger BV, and Dimigen O (2019). Unfold: an integrated toolbox for overlap correction, non-linear modeling, and regression-based EEG analysis. PeerJ 7, e7838. [PubMed: 31660265]

Elward RL, Rugg MD, and Vargha-Khadem F (2021). When the brain, but not the person, remembers: cortical reinstatement is modulated by retrieval goal in developmental amnesia. Neuropsychologia 154, 107788. [PubMed: 33587931]

Fernández-Ruiz A, Oliva A, de Oliveira EF, Rocha-Almeida F, Tingley D, and Buzsáki G (2019). Long-duration hippocampal sharp wave ripples improve memory. Science 364, 1082–1086. [PubMed: 31197012]

Fiederer LD, Lahr J, Vorwerk J, Lucka F, Aertsen A, Wolters CH, Schulze-Bonhage A, and Ball T (2016). Electrical Stimulation of the Human Cerebral Cortex by Extracranial Muscle Activity: Effect Quantification With Intracranial EEG and FEM Simulations. IEEE Trans. Biomed. Eng 63, 2552–2563. [PubMed: 27448334]

Fischl B (2012). FreeSurfer. Neuroimage 62, 774–781. [PubMed: 22248573]

Foster DJ, and Wilson MA (2006). Reverse replay of behavioural sequences in hippocampal place cells during the awake state. Nature 440, 680–683. [PubMed: 16474382]

Foster BL, Rangarajan V, Shirer WR, and Parvizi J (2015). Intrinsic and task-dependent coupling of neuronal population activity in human parietal cortex. Neuron 86, 578–590. [PubMed: 25863718]

Fox KCR, Foster BL, Kucyi A, Daitch AL, and Parvizi J (2018). Intracranial Electrophysiology of the Human Default Network. Trends Cogn. Sci 22, 307–324. [PubMed: 29525387]

Gelbard-Sagiv H, Mukamel R, Harel M, Malach R, and Fried I (2008). Internally generated reactivation of single neurons in human hippocampus during free recall. Science 322, 96–101. [PubMed: 18772395]

Gelinas JN, Khodagholy D, Thesen T, Devinsky O, and Buzsáki G (2016). Interictal epileptiform discharges induce hippocampal-cortical coupling in temporal lobe epilepsy. Nat. Med 22, 641–648. [PubMed: 27111281]

Gilboa A, Winocur G, Grady CL, Hevenor SJ, and Moscovitch M (2004). Remembering our past: functional neuroanatomy of recollection of recent and very remote personal events. Cereb. Cortex 14, 1214–1225. [PubMed: 15166099]

Girardeau G, Benchenane K, Wiener SI, Buzsáki G, and Zugaro MB (2009). Selective suppression of hippocampal ripples impairs spatial memory. Nat. Neurosci 12, 1222–1223. [PubMed: 19749750]

Girardeau G, Inema I, and Buzsáki G (2017). Reactivations of emotional memory in the hippocampus-amygdala system during sleep. Nat. Neurosci 20, 1634–1642. [PubMed: 28892057]

Golan T, Davidesco I, Meshulam M, Groppe DM, Mégevand P, Yeagle EM, Goldfinger MS, Harel M, Melloni L, Schroeder CE, et al. (2016). Human intracranial recordings link suppressed transients rather than 'filling-in' to perceptual continuity across blinks. eLife 5, e17243. [PubMed: 27685352]

Gomperts SN, Kloosterman F, and Wilson MA (2015). VTA neurons coordinate with the hippocampal reactivation of spatial experience. eLife 4, 1–22.

Groppe DM, Urbach TP, and Kutas M (2011). Mass univariate analysis of event-related brain potentials/fields I: a critical tutorial review. Psychophysiology 48, 1711–1725. [PubMed: 21895683]

Groppe DM, Bickel S, Dykstra AR, Wang X, Mégevand P, Mercier MR, Lado FA, Mehta AD, and Honey CJ (2017). iELVis: an open source MATLAB toolbox for localizing and visualizing human intracranial electrode data. J. Neurosci. Methods 287, 40–48.

Hamilton JP, Farmer M, Fogelman P, and Gotlib IH (2015). Depressive Rumination, the Default-Mode Network, and the Dark Matter of Clinical Neuroscience. Biol. Psychiatry 78, 224–230. [PubMed: 25861700]

Harmelech T, Friedman D, and Malach R (2015). Differential magnetic resonance neurofeedback modulations across extrinsic (visual) and intrinsic (default-mode) nodes of the human cortex. J. Neurosci 35, 2588–2595. [PubMed: 25673851]

Helfrich RF, Lendner JD, Mander BA, Guillen H, Paff M, Mnatsakanyan L, Vadera S, Walker MP, Lin JJ, and Knight RT (2019). Bidirectional prefrontal-hippocampal dynamics organize information transfer during sleep in humans. Nat. Commun 10, 3572. [PubMed: 31395890]

Henin S, Shankar A, Borges H, Flinker A, Doyle W, Friedman D, Devinsky O, Buzsáki G, and Liu A (2021). Spatiotemporal dynamics between interictal epileptiform discharges and ripples during associative memory processing. Brain 144, 1590–1602. [PubMed: 33889945]

Hentschke H, and Stüttgen MC (2011). Computation of measures of effect size for neuroscience data sets. Eur. J. Neurosci 34, 1887–1894. [PubMed: 22082031]

Higgins C, Liu Y, Vidaurre D, Kurth-Nelson Z, Dolan R, Behrens T, and Woolrich M (2021). Replay bursts in humans coincide with activation of the default mode and parietal alpha networks. Neuron 109, 882–893.e7. [PubMed: 33357412]

Iglesias JE, Augustinack JC, Nguyen K, Player CM, Player A, Wright M, Roy N, Frosch MP, McKee AC, Wald LL, et al. ; Alzheimer's Disease Neuroimaging Initiative (2015). A computational atlas of the hippocampal formation using exvivo, ultra-high resolution MRI: application to adaptive segmentation of in vivo MRI. Neuroimage 115, 117–137. [PubMed: 25936807]

Jadhav SP, Kemere C, German PW, and Frank LM (2012). Awake Hippocampal Sharp-Wave Ripples Support Spatial Memory. Science 336, 1454–1458. [PubMed: 22555434]

Joo HR, and Frank LM (2018). The hippocampal sharp wave-ripple in memory retrieval for immediate use and consolidation. Nat. Rev. Neurosci 19, 744–757. [PubMed: 30356103]

Kaplan R, Adhikari MH, Hindriks R, Mantini D, Murayama Y, Logothetis NK, and Deco G (2016). Hippocampal Sharp-Wave Ripples Influence Selective Activation of the Default Mode Network. Curr. Biol 26, 686–691. [PubMed: 26898464]

Karimi Abadchi J, Nazari-Ahangarkolaee M, Gattas S, Bermudez-Contreras E, Luczak A, McNaughton BL, and Mohajerani MH (2020). Spatiotemporal patterns of neocortical activity around hippocampal sharp-wave ripples. eLife 9, 1–26.

Karlsson MP, and Frank LM (2009). Awake replay of remote experiences in the hippocampus. Nat. Neurosci 12, 913–918. [PubMed: 19525943]

Kartsounis LD, Rudge P, and Stevens JM (1995). Bilateral lesions of CA1 and CA2 fields of the hippocampus are sufficient to cause a severe amnesic syndrome in humans. J. Neurol. Neurosurg. Psychiatry 59, 95–98. [PubMed: 7608720]

Kim H (2010). Dissociating the roles of the default-mode, dorsal, and ventral networks in episodic memory retrieval. Neuroimage 50, 1648–1657. [PubMed: 20097295]

Lenth RV (2016). Least-Squares Means: The R Package lsmeans. J. Stat. Softw 69, 1–33.

Leonard TK, and Hoffman KL (2017). Sharp-Wave Ripples in Primates Are Enhanced near Remembered Visual Objects. Curr. Biol 27, 257–262. [PubMed: 28041797]

Li X, Liang Z, Kleiner M, and Lu ZL (2010). RTbox: a device for highly accurate response time measurements. Behav. Res. Methods 42, 212–225. [PubMed: 20160301]

Liu S, and Parvizi J (2019). Cognitive refractory state caused by spontaneous epileptic high-frequency oscillations in the human brain. Sci. Transl. Med 11, 1–14.

Liu S, Sha Z, Sencer A, Aydoseli A, Bebek N, Abosch A, Henry T, Gurses C, and Ince NF (2016). Exploring the time-frequency content of high frequency oscillations for automated identification of seizure onset zone in epilepsy. J. Neural Eng 13, 026026. [PubMed: 26924828]

Logothetis NK, Eschenko O, Murayama Y, Augath M, Steudel T, Evrard HC, Besserve M, and Oeltermann A (2012). Hippocampal-cortical interaction during periods of subcortical silence. Nature 491, 547–553. [PubMed: 23172213]

Maguire EA (2001). Neuroimaging studies of autobiographical event memory. Philos. Trans. R. Soc. Lond. B Biol. Sci 356, 1441–1451. [PubMed: 11571035]

Maguire EA, and Frith CD (2003). Lateral asymmetry in the hippocampal response to the remoteness of autobiographical memories. J. Neurosci 23, 5302–5307. [PubMed: 12832555]

Maingret N, Girardeau G, Todorova R, Goutierre M, and Zugaro M (2016). Hippocampo-cortical coupling mediates memory consolidation during sleep. Nat. Neurosci 19, 959–964. [PubMed: 27182818]

Maris E, and Oostenveld R (2007). Nonparametric statistical testing of EEG-and MEG-data. J. Neurosci. Methods 164, 177–190. [PubMed: 17517438]

McClelland JL, McNaughton BL, and O'Reilly RC (1995). Why there are complementary learning systems in the hippocampus and neocortex: insights from the successes and failures of connectionist models of learning and memory. Psychol. Rev 102, 419–457. [PubMed: 7624455]

McCormick C, Moscovitch M, Valiante TA, Cohn M, and McAndrews MP (2018). Different neural routes to autobiographical memory recall in healthy people and individuals with left medial temporal lobe epilepsy. Neuropsychologia 110, 26–36. [PubMed: 28803766]

McCormick C, Barry DN, Jafarian A, Barnes GR, and Maguire EA (2020). vmPFC Drives Hippocampal Processing during Autobiographical Memory Recall Regardless of Remoteness. Cereb. Cortex 30, 5972–5987. [PubMed: 32572443]

Moscovitch M, Rosenbaum RS, Gilboa A, Addis DR, Westmacott R, Grady C, McAndrews MP, Levine B, Black S, Winocur G, and Nadel L (2005). Functional neuroanatomy of remote episodic, semantic and spatial memory: a unified account based on multiple trace theory. J. Anat 207, 35–66. [PubMed: 16011544]

Moscovitch M, Cabeza R, Winocur G, and Nadel L (2016). Episodic memory and beyond: the hippocampus and neocortex in transformation. Annu. Rev. Psychol 67, 105–134. [PubMed: 26726963]

Mukamel R, Gelbard H, Arieli A, and Hasson U (2005). Coupling Between Neuronal Firing, Field Potentials, and fMRI in Human Auditory Cortex. Science 300,951–954.

Nadel L, and Moscovitch M (1997). Memory consolidation, retrograde amnesia and the hippocampal complex. Curr. Opin. Neurobiol 7, 217–227. [PubMed: 9142752]

Ngo HV, Fell J, and Staresina B (2020). Sleep spindles mediate hippocampal-neocortical coupling during long-duration ripples. eLife 9, 1–18.

Norman Y, Yeagle EM, Harel M, Mehta AD, and Malach R (2017). Neuronal baseline shifts underlying boundary setting during free recall. Nat. Commun 8, 1301. [PubMed: 29101322]

Norman Y, Yeagle EMEM, Khuvis S, Harel M, Mehta ADAD, and Malach R (2019). Hippocampal sharp-wave ripples linked to visual episodic recollection in humans. Science 365, eaax1030. [PubMed: 31416934]

O'Reilly RC, Bhattacharyya R, Howard MD, and Ketz N (2014). Complementary learning systems. Cogn. Sci 38, 1229–1248. [PubMed: 22141588]

Oliva A, Fernández-Ruiz A, Buzsáki G, and Berényi A (2016). Role of Hippocampal CA2 Region in Triggering Sharp-Wave Ripples. Neuron 91, 1342–1355. [PubMed: 27593179]

Oliva A, Fernández-Ruiz A, Leroy F, and Siegelbaum SA (2020). Hippocampal CA2 sharp-wave ripples reactivate and promote social memory. Nature 587, 264–269. [PubMed: 32968277]

OpenWetWare (2015). Mass Univariate ERP Toolbox. https://openwetware.org/wiki/Mass_Univariate_ERP_Toolbox.

Papademetris X, Jackowski MP, Rajeevan N, DiStasio M, Okuda H, Constable RT, and Staib LH (2006). BioImage Suite: an integrated medical image analysis suite: an update. Insight J. 2006, 209. [PubMed: 25364771]

Parvizi J, and Kastner S (2018). Promises and limitations of human intracranial electroencephalography. Nat. Neurosci 21, 474–483. [PubMed: 29507407]

Patel J, Schomburg EW, Berényi A, Fujisawa S, and Buzsáki G (2013). Local generation and propagation of ripples along the septotemporal axis of the hippocampus. J. Neurosci 33, 17029–17041. [PubMed: 24155307]

Peyrache A, Khamassi M, Benchenane K, Wiener SI, and Battaglia FP (2009). Replay of rule-learning related neural patterns in the prefrontal cortex during sleep. Nat. Neurosci 12, 919–926. [PubMed: 19483687]

Quiroga RQ (2012). Concept cells: the building blocks of declarative memory functions. Nat. Rev. Neurosci 13, 587–597. [PubMed: 22760181]

Quiroga RQ (2019). Plugging in to Human Memory: Advantages, Challenges, and Insights from Human Single-Neuron Recordings. Cell 179, 1015–1032. [PubMed: 31730847]

Quiroga RQ, Reddy L, Kreiman G, Koch C, and Fried I (2005). Invariant visual representation by single neurons in the human brain. Nature 435, 1102–1107. [PubMed: 15973409]

R Core Development Team (2017). R: A language and environment for statistical computing (R Foundation for Statistical Computing).

Raccah O, Daitch AL, Kucyi A, and Parvizi J (2018). Direct cortical recordings suggest temporal order of task-evoked responses in human dorsal attention and default networks. J. Neurosci 38, 10305–10313. [PubMed: 30315126]

Raichle ME (2015). The brain's default mode network. Annu. Rev. Neurosci 38, 433–447. [PubMed: 25938726]

Rajasethupathy P, Sankaran S, Marshel JH, Kim CK, Ferenczi E, Lee SY, Berndt A, Ramakrishnan C, Jaffe A, Lo M, et al. (2015). Projections from neocortex mediate top-down control of memory retrieval. Nature 526, 653–659. [PubMed: 26436451]

Renoult L, Irish M, Moscovitch M, and Rugg MD (2019). From Knowing to Remembering: The Semantic-Episodic Distinction. Trends Cogn. Sci 23, 1041–1057. [PubMed: 31672430]

Robin J, and Moscovitch M (2017). Details, gist and schema: hippocampal–neocortical interactions underlying recent and remote episodic and spatial memory. Curr. Opin. Behav. Sci 17, 114–123.

Rosenbaum RS, Priselac S, Köhler S, Black SE, Gao F, Nadel L, and Moscovitch M (2000). Remote spatial memory in an amnesic person with extensive bilateral hippocampal lesions. Nat. Neurosci 3, 1044–1048. [PubMed: 11017178]

Rothschild G, Eban E, and Frank LM (2017). A cortical-hippocampalcortical loop of information processing during memory consolidation. Nat. Neurosci 20, 251–259. [PubMed: 27941790]

Rutishauser U, Reddy L, Mormann F, and Sarnthein J (2021). The Architecture of Human Memory: Insights from Human Single-Neuron Recordings. J. Neurosci 41, 883–890. [PubMed: 33257323]

Ryan L, Nadel L, Keil K, Putnam K, Schnyer D, Trouard T, and Moscovitch M (2001). Hippocampal complex and retrieval of recent and very remote autobiographical memories: evidence from functional magnetic resonance imaging in neurologically intact people. Hippocampus 11,707–714. [PubMed: 11811665]

Saad ZS, and Reynolds RC (2012). Suma. Neuroimage 62, 768–773. [PubMed: 21945692]

Schacter DL, Addis DR, Hassabis D, Martin VC, Spreng RN, and Szpunar KK (2012). The future of memory: remembering, imagining, and the brain. Neuron 76, 677–694. [PubMed: 23177955]

Scoville WB, and Milner B (1957). Loss of recent memory after bilateral hippocampal lesions. J. Neurol. Neurosurg. Psychiatry 20, 11–21. [PubMed: 13406589]

Seheult AH, and Green PJ (1989). Review: Robust Regression and Outlier Detection by P. J. Rousseeuw, A. M. Leroy. J. R. Stat. Soc 152, 133–134.

Sekeres MJ, Winocur G, and Moscovitch M (2018). The hippocampus and related neocortical structures in memory transformation. Neurosci. Lett 680, 39–53. [PubMed: 29733974]

Shin JD, Tang W, and Jadhav SP (2019). Dynamics of Awake Hippocampal-Prefrontal Replay for Spatial Learning and Memory-Guided Decision Making. Neuron 104, 1110–1125.e7. [PubMed: 31677957]

Singmann H, Bolker B, Westfall J, Aust F, and Ben-Shachar MS (2020). afex: analysis of factorial experiments. https://cran.r-project.org/web/packages/afex/index.html.

Squire LR, and Zola SM (1996). Structure and function of declarative and nondeclarative memory systems. Proc. Natl. Acad. Sci. USA 93, 13515–13522. [PubMed: 8942965]

Squire LR, Stark CEL, and Clark RE (2004). The medial temporal lobe. Annu. Rev. Neurosci 27, 279–306. [PubMed: 15217334]

Squire LR, Genzel L, Wixted JT, and Morris RG (2015). Memory consolidation. Cold Spring Harb. Perspect. Biol 7, a021766. [PubMed: 26238360]

Staresina BP, Bergmann TO, Bonnefond M, van der Meij R, Jensen O, Deuker L, Elger CE, Axmacher N, and Fell J (2015). Hierarchical nesting of slow oscillations, spindles and ripples in the human hippocampus during sleep. Nat. Neurosci 18, 1679–1686. [PubMed: 26389842]

Staresina BP, Reber TP, Niediek J, Boström J, Elger CE, and Mormann F (2019). Recollection in the human hippocampal-entorhinal cell circuitry. Nat. Commun 10, 1503. [PubMed: 30944325]

Takahashi S (2015). Episodic-like memory trace in awake replay of hippocampal place cell activity sequences. eLife 4, e08105. [PubMed: 26481131]

Todorova R, and Zugaro M (2020). Hippocampal ripples as a mode of communication with cortical and subcortical areas. Hippocampus 30, 39–49. [PubMed: 30069976]

Tulving E (2002). Episodic memory: from mind to brain. Annu. Rev. Psychol 53, 1–25. [PubMed: 11752477]

Tulving E, and Markowitsch HJ (1998). Episodic and declarative memory: role of the hippocampus. Hippocampus 8, 198–204. [PubMed: 9662134]

van de Ven GM, Trouche S, McNamara CG, Allen K, and Dupret D (2016). Hippocampal Offline Reactivation Consolidates Recently Formed Cell Assembly Patterns during Sharp Wave-Ripples. Neuron 92, 968–974. [PubMed: 27840002]

Van Der Maaten LJP, Postma EO, and Van Den Herik HJ (2009). Dimensionality Reduction: A Comparative Review. J. Mach. Learn. Res 10, 1–41.

Vargha-Khadem F, Gadian DG, Watkins KE, Connelly A, Van Paesschen W, Mishkin M, Van Paesschen W, and Mishkin M (1997). Differential effects of early hippocampal pathology on episodic and semantic memory. Science 277, 376–380. [PubMed: 9219696]

Vatansever D, Smallwood J, and Jefferies E (2021). Varying demands for cognitive control reveals shared neural processes supporting semantic and episodic memory retrieval. Nat. Commun 12, 2134. [PubMed: 33837220]

Vaz AP, Inati SK, Brunel N, and Zaghloul KA (2019). Coupled ripple oscillations between the medial temporal lobe and neocortex retrieve human memory. Science 363, 975–978. [PubMed: 30819961]

Vaz AP, Wittig JH, Inati SK, and Zaghloul KA (2020). Replay of cortical spiking sequences during human memory retrieval. Science 367, 1131–1134. [PubMed: 32139543]

Viard A, Piolino P, Desgranges B, Chételat G, Lebreton K, Landeau B, Young A, De La Sayette V, and Eustache F (2007). Hippocampal activation for autobiographical memories over the entire lifetime in healthy aged subjects: an fMRI study. Cereb. Cortex 17, 2453–2467. [PubMed: 17204823]

Watson BO, Ding M, and Buzsáki G (2018). Temporal coupling of field potentials and action potentials in the neocortex. Eur. J. Neurosci 48, 2482–2497. [PubMed: 29250852]

Winocur G, and Moscovitch M (2011). Memory transformation and systems consolidation. J. Int. Neuropsychol. Soc 17, 766–780. [PubMed: 21729403]

Wu CT, Haggerty D, Kemere C, and Ji D (2017). Hippocampal awake replay in fear memory retrieval. Nat. Neurosci 20, 571–580. [PubMed: 28218916]

Yeo BT, Krienen FM, Sepulcre J, Sabuncu MR, Lashkari D, Hollinshead M, Roffman JL, Smoller JW, Zöllei L, Polimeni JR, et al. (2011). The organization of the human cerebral cortex estimated by intrinsic functional connectivity. J. Neurophysiol 106, 1125–1165. [PubMed: 21653723]

Zhang H, Fell J, and Axmacher N (2018). Electrophysiological mechanisms of human memory consolidation. Nat. Commun 9, 4103. [PubMed: 30291240]

Highlights

- Simultaneous iEEG recordings of cortex and hippocampal ripples linked to cognition
- Ripples selectively activate during autobiographic and semantic memory recall
- Multisite ripple activity patterns reflect memory semantization processes
- Ripples coordinate a DMN-centered cortical-hippocampal interplay during recall

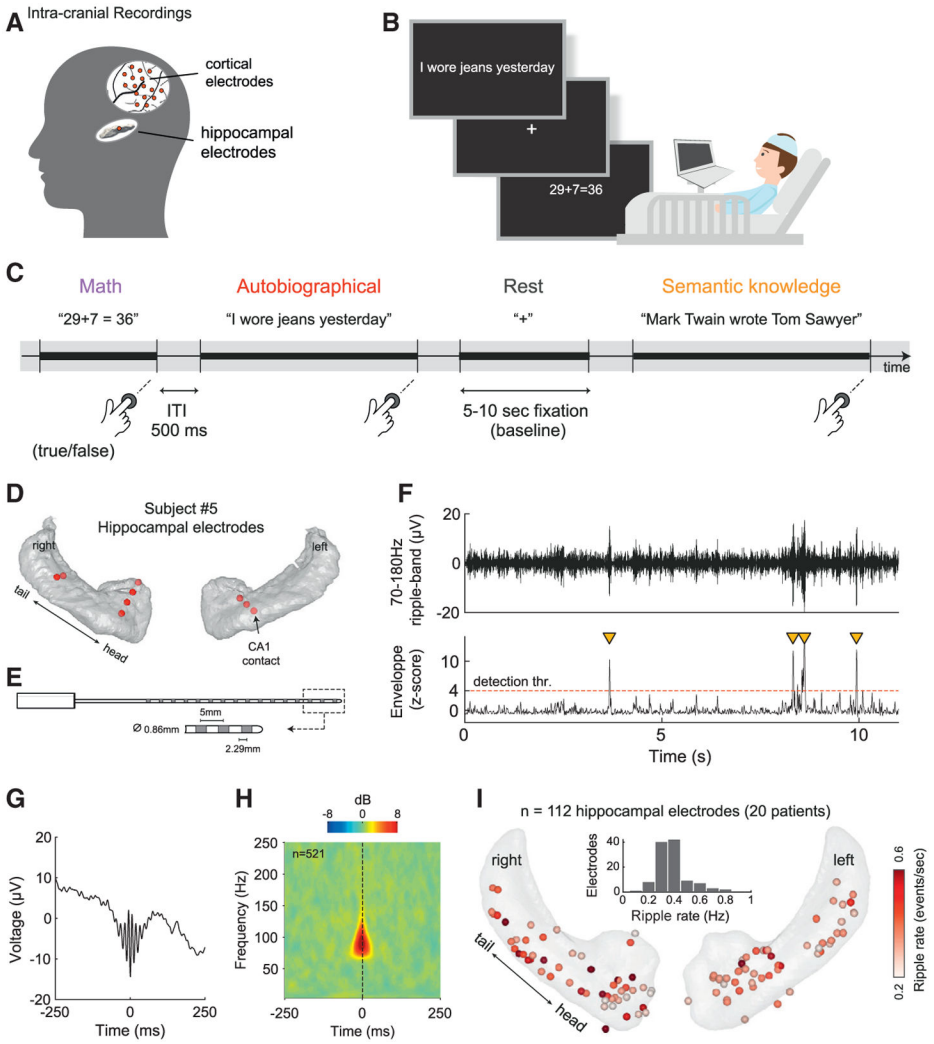

Figure 1. Experimental design, intracranial recordings, and ripple detection

(A) Intracranial electrodes were implanted in the hippocampus and cortex as part of a neurosurgical treatment for medically intractable epilepsy.

(B and C) Participants were instructed to make true/false judgments about a series of visually presented statements, requiring either autobiographical memory (autobio), arithmetic processing, or semantic knowledge (in a subgroup of 11 subjects).

(D) Hippocampal electrodes in 1 example patient. Red circles indicate recording sites where ripples were detected. To see the map of hippocampal coverage across all subjects, see (I).

(E) Schematic diagram of a typical depth iEEG electrode used in our study (see also Table S3).

(F) Example of hippocampal ripples as they appear in a CA1 recording site (see black arrow in D). Orange triangles mark ripple events that met the detection criteria (see STAR Methods).

(G and H) Mean peri-ripple field potential and wavelet spectrogram for the same CA1 site described in (F), showing the typical spectrotemporal signature of human hippocampal ripples (n = 521 ripples, peak frequency: 94 ± 1.71 Hz).

(I) Overview of ripple rate computed over the entire experiment, for each hippocampal site included in our analysis (112 sites from 20 patients). Inset: distribution of ripple rates across electrodes.

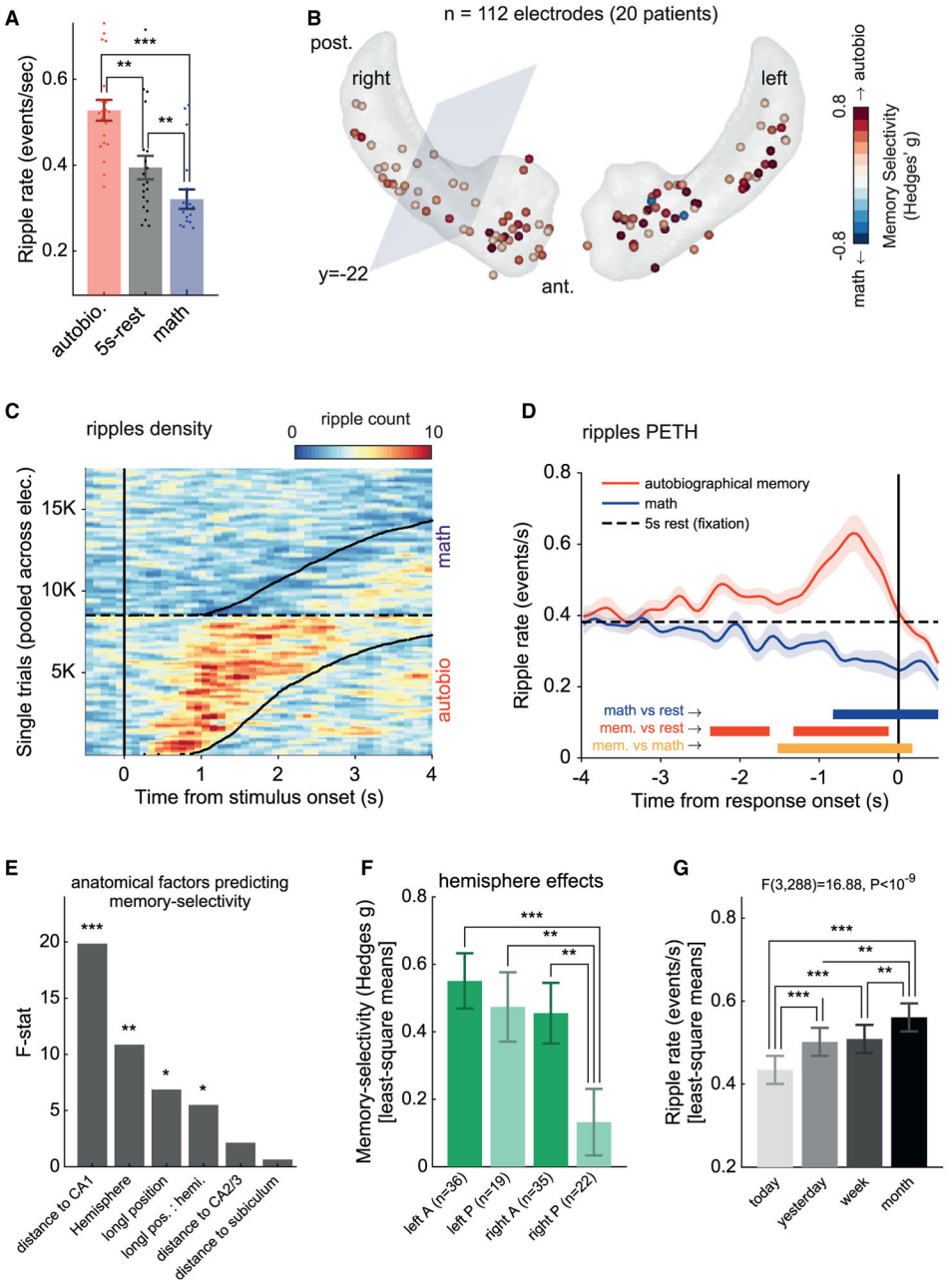

Figure 2. Ripple rate modulation during autobiographical retrieval compared to arithmetic processing

(A) Group results showing mean ripple rate across the main experimental conditions: autobiographical memory, arithmetic processing, and 5-s rest intervals (fixation). Filled dots represent individual patients. Error bars represent SEM across patients (n = 20).

(B) Schematic depiction of hippocampal recording sites on a hippocampus template in Montreal Neurological Institute (MNI) space. Electrodes were color-coded according to their memory selectivity (autobiographical versus math, bias-corrected Hedges's g effect size). Positive values (red) indicate a higher ripple rate during autobiographical retrieval

compared to math. The anterior hippocampus was defined as the region having an MNI y coordinate of<–22 (ensuring complete coverage of the uncus).

(C) Hippocampal ripples density plot showing increase/decrease in ripple probability following autobiographical and math statements, respectively. Trials were pooled together across all electrodes and sorted according to reaction time (black curve). Ripples' density was computed in bins of 100 ms × 100 trials, smoothed using a 3-bins-wide Gaussian filter for visualization purposes. Note that the transient increases in ripple probability closely tracked reaction times.

(D) Group-level analysis showing the average peri-event time histogram (PETH) of ripples, time-locked to the reaction time (using 50-ms-wide bins). There was a significant decrease in ripple rate during math (blue) and a significant increase during autobiographical retrieval (red), peaking 600 ms before the patient's response. Shaded area represents SEM across patients (n = 20).

(E and F) Mixed effects analysis of the autobio-versus-math contrast across recording sites revealed significant effects of "CA1 distance" ($F(1,82.90) = 19.38$, $p < 3.17 \times 10^{-5}$) and "hemisphere" ($F(1,93.01) = 10.17$, $p = 0.0019$), as well as an interaction between "hemisphere" and "longitudinal position" ($F(1,83.68) = 5.30$, $p = 0.023$). Thus, memory selectivity was significantly stronger in electrodes closer to CA1 and in electrodes located in the left hippocampus. Post hoc 2-sample t tests further indicated that the right posterior hippocampus showed the weakest memory selectivity (*p < 0.05, **p < 0.01, ***p < 0.001; FDR corrected). Error bars represent SEM.

(G) A mixed-effects analysis of ripple rates elicited during the autobiographical trials revealed a significant effect of memory age ($F(3,288) = 18.27$, $p < 10^{-10}$; n = 16 patients). Post hoc comparisons indicated that retrieval of remote memories elicited higher ripple rates compared to more recent memories (*p < 0.05, **p < 0.01, ***p < 0.001; FDR corrected). Error bars represent SEM.

See also Figure S2.

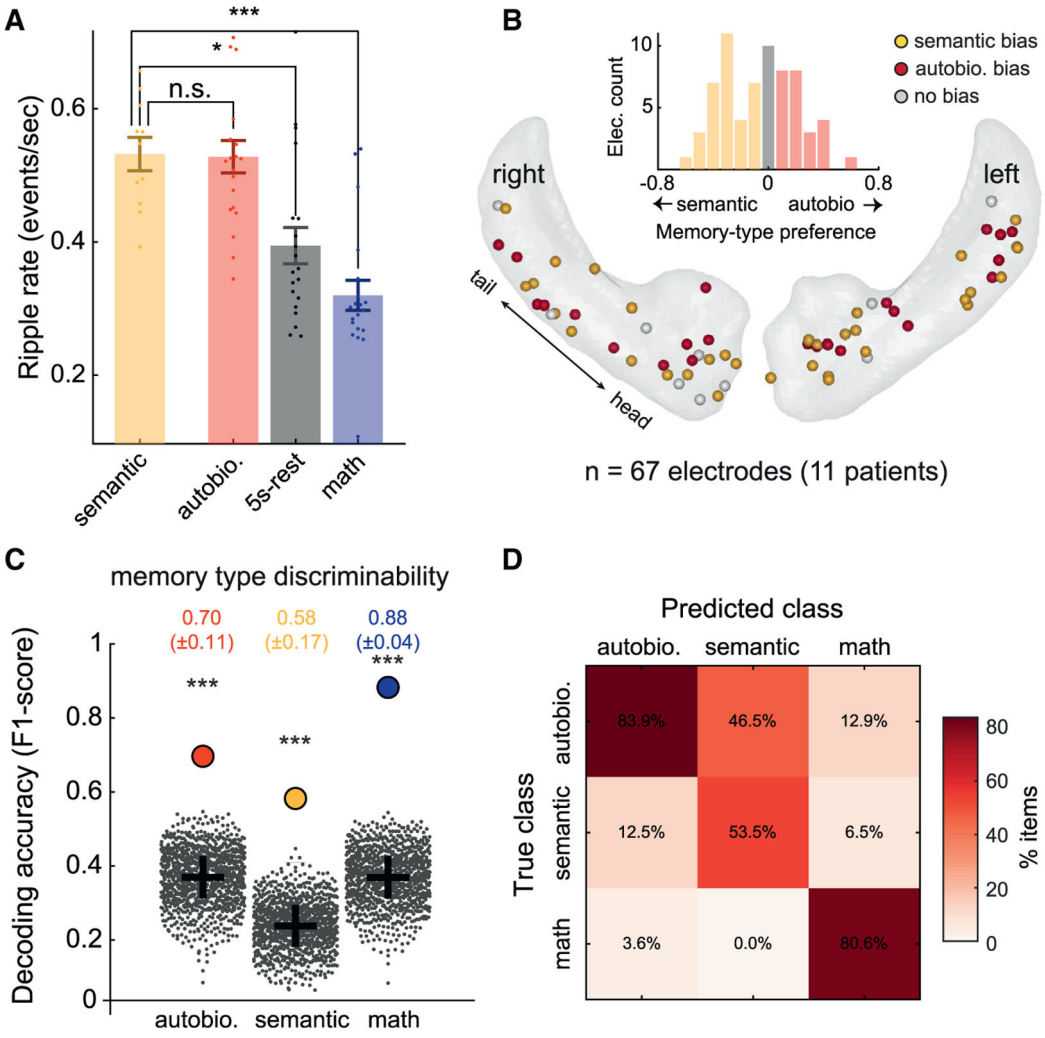

Figure 3. Multisite patterns of ripples discriminate between autobiographical and semantic memory

(A) Averaging over electrodes within a subject and comparing overall ripple rates across conditions using partially overlapping samples t tests (Derrick et al., 2017) showed no significant difference between autobio and semantic memory ($t(14.51) = 0.17$, $p > 0.87$). Similar to the autobio condition, the semantic condition elicited higher ripple rates compared to both math ($t(14.17) = 5.27$, $p < 0.001$) and 5-s rest ($t(15.06) = 2.98$, $p < 0.01$). Error bars represent SEM.

(B) Schematic depiction of the recording sites' functional specialization in MNI space, showing a mixed and balanced spatial distribution of memory-type biases. Inset: effect size histogram of the autobiographical versus semantic bias at individual sites, pointing to the absence of clear functional segregation between memory types. Electrodes marked in red or yellow showed a slight bias for autobio or semantic memory, respectively.

(C) Linear discriminant analysis (LDA) classifier trained to decode trial type from multivariate ripple rate patterns (computed across all electrodes pooled together) significantly discriminated between semantic and autobiographical trials. Decoding performance was quantified using F1 score: autobio, 0.70 ± 0.11; semantic, 0.58 ± 0.17;

math, 0.88 ± 0.04 (SEM was computed using a jackknife procedure, excluding 1 patient at a time). Filled circles denote the actual results; gray dots show results for same data when trial labels were randomly shuffled; gray crosses indicate the chance level in each class (different due to the different number of items in each class).

(D) Confusion matrix showing that classification errors were primarily due to confusion between autobiographical and semantic trials.

See also Figure S4.

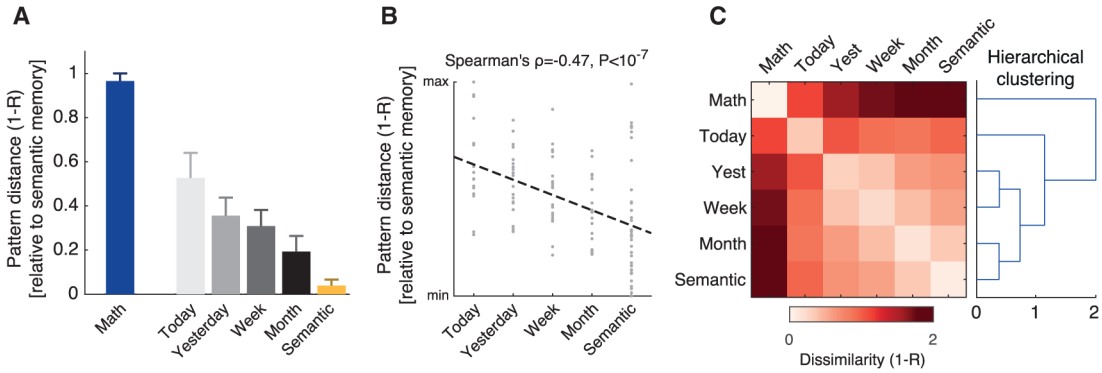

Figure 4. Ripple activity pattern similarity reflects memory semantization

(A) Distance (dissimilarity) between the average pattern during semantic trials and the average patterns emerging during the 4 memory age categories of autobiographical trials (i.e., statements referring to “today,” “yesterday,” “this week,” and “last month”). Note the growing resemblance between autobiographical and semantic patterns as memories become more remote. Error bars represent bootstrap SE.

(B) The distances (dissimilarity) between ripple rate patterns associated with individual memory items and the average semantic pattern showed a significant negative correlation with memory age (Spearman’s $\rho = -0.47$, $p < 10^{-7}$, n = 115 memory items; dashed line is the least-squares line). Thus, the more remote the autobiographical memory was, the more similar its associated ripple rate pattern was to semantic memory.

(C) Agglomerative hierarchical clustering (using group-average linkage) applied to the average ripple rate patterns of the different conditions reveals that multisite ripple activity forms a hierarchy of pattern similarity that reflects the episodic-semantic continuum.

See also Figure S4.

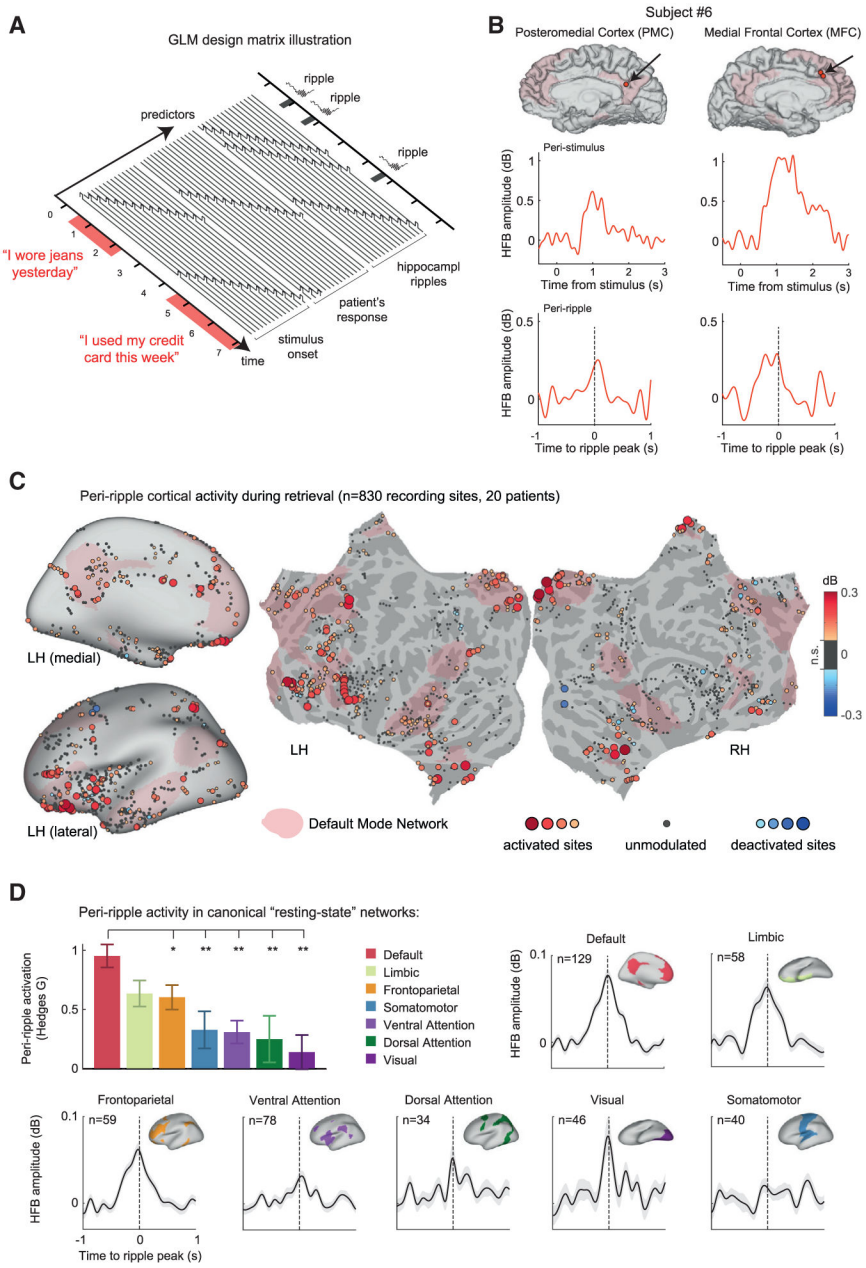

Figure 5. Peri-ripple cortical activations during autobiographical recall

(A) A schematic illustration of the general linear model (GLM) design matrix used in the deconvolution of peri-ripple cortical responses. The observed HFB time series in each cortical site was modeled as a linear sum of overlapping responses triggered by stimulus-presentation, hippocampal ripple events, and the patient's reaction. Each of these experimental events was entered into the model as a sequence of semi-overlapping cubic splines basis functions, which allowed the isolation of the peri-ripple activation while accounting for the activity induced by the other experimental events.

(B) Representative signal from two cortical sites in a single patient showing deconvolved stimulus-related (center row) and ripple-related HFB responses (bottom row). Hippocampal ripple time stamps taken from a single CA1 site in the same subject.
(C) Cortical electrodes (bipolar pairs) colored according to their deconvolved peri-ripple HFB response during the autobiographical trials. HFB amplitude was averaged over a time-window of −250 to 250 ms relative to the hippocampal ripple peak. Peri-ripple activations were broadly distributed, implicating prefrontal regions and large portions of the medial cortical surface overlapping the DMN (pink-colored regions). The threshold for electrode visualization was determined based on comparison to a null distribution of peri-ripple HFB responses, computed using a time-window of −1,500 to −500 ms relative to the ripple event. Recording sites in which the actual peri-ripple response failed to cross a threshold of $p < 0.05$ (uncorrected) were regarded as ripple-unmodulated sites and colored in gray.
(D) Peri-ripple activations across seven canonical resting-state networks, based on the Yeo et al. (2011) atlas. The bar plot shows that peri-ripple HFB amplitude in DMN electrodes, averaged over a time window of −250 to 250 ms relative to ripple peak, was significantly stronger compared to the other networks (*$p < 0.05$, **$p < 0.01$, rank-sum test, FDR adjusted; “limbic” sites were non-significantly different from DMN). In this analysis, we required that both electrodes in the bipolar pair be located within the affiliated resting-state network, thus achieving better anatomical specificity. Error bars represent SEM across recording sites.
See also Figures S5 and S6.

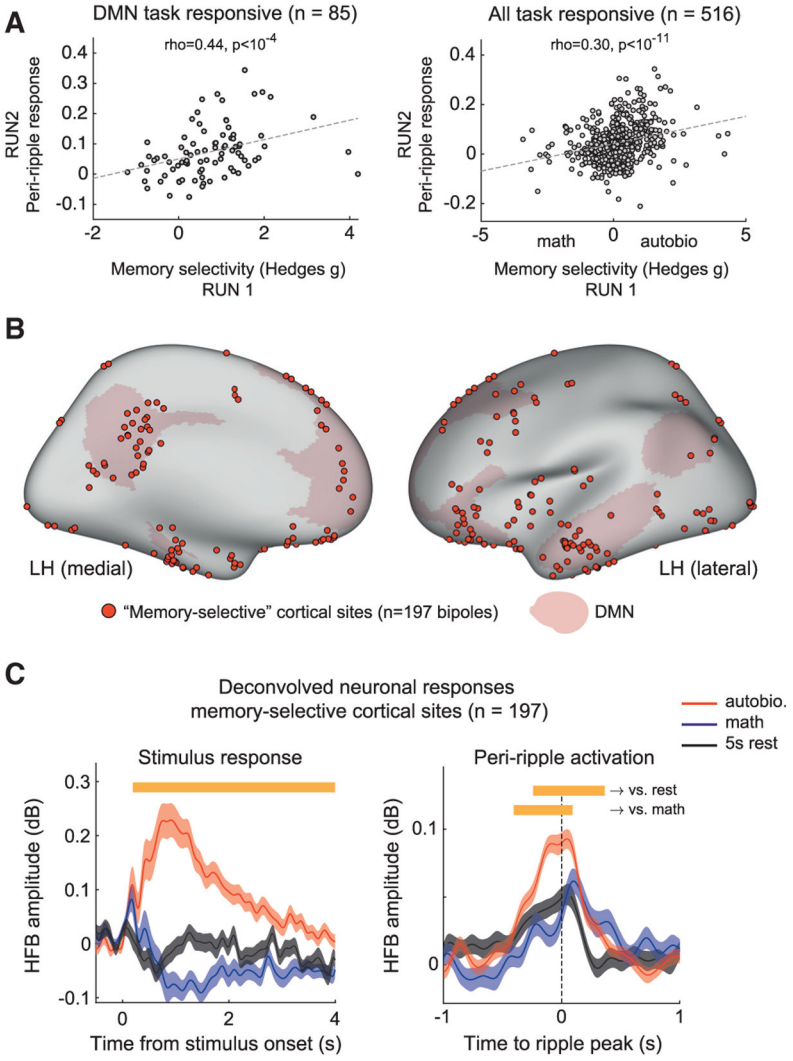

Figure 6. Peri-ripple response across memory-selective sites in the cortex

(A) Correlation between memory selectivity (defined as the standardized difference in HFB stimulus response between autobio and math conditions) and the magnitude of peri-ripple activation, in task-responsive sites located within the DMN (left; Spearman's $\rho = 0.44$, $p < 10^{-4}$, n = 85 sites) and across the entire cortex (right; Spearman's $\rho = 0.3$, $p < 10^{-11}$, n = 516 sites)..

(B) Anatomical distribution of memory-selective cortical sites (red circles; see STAR Methods).

(C) Deconvolved stimulus-related and peri-ripple HFB activity averaged across all memory-selective cortical sites (n = 197 bipoles). Peri-ripple response was significantly stronger during autobiographical trials compared to math or rest ($p < 0.001$, cluster-based permutation test). Shaded areas represent SEM.

See also Figure S6.

KEY RESOURCES TABLE

REAGENT or RESOURCE	SOURCE	IDENTIFIER
Software and algorithms		
EEGLAB v14.1.2.	Delorme and Makeig, 2004	https://sccn.ucsd.edu/eeglab/index.php
DRtoolbox	Van Der Maaten et al., 2009	https://lvdmaaten.github.io/drtoolbox/
MES toolbox	Hentschke and Stfittgen, 2011	https://github.com/hhentschke/measures-of-effect-size-toolbox
Unfold 1.1 EEG Deconvolution Toolbox	Ehinger and Dimigen, 2019	https://www.unfoldtoolbox.org/
iELVis toolbox	Groppe et al., 2017	http://ielvis.pbworks.com/w/page/116347253/FrontPage
Mass Univariate ERP Toolbox	Groppe et al., 2011	https://openwetware.org/wiki/Mass_Univariate_ERP_Toolbox
SUMA	Saad and Reynolds, 2012	https://afni.nimh.nih.gov/pub/dist/doc/htmldoc/SUMA/main_toc.html
Custom-developed analysis code	N/A	https://doi.org/10.5281/zenodo.4759103
Deposited Data	N/A	https://doi.org/10.5281/zenodo.4759103